The impact of supraglacial debris on proglacial runoff and water chemistry

Fyffe, C. L.[a], Brock, B. W.[a], Kirkbride, M. P.[b], Black, A. R.[b], Smiraglia, C.[c] and Diolaiuti, G.[c]

[a] catriona.fyffe@northumbria.ac.uk (corresponding author), +44(0)191 227 3956, and benjamin.brock@northumbria.ac.uk, Department of Geography and Environmental Sciences, Northumbria University, Newcastle-Upon-Tyne, United Kingdom

[b] m.p.kirkbride@dundee.ac.uk and a.z.black@dundee.ac.uk, School of the Environment, University of Dundee, Dundee, United Kingdom

[c] claudio.smiraglia@unimi.it and guglielmina.diolaiuti@unimi.it, Department of Earth Sciences 'Ardito Desio', University of Milan, Milan, Italy

Abstract

Debris is known to influence the ablation, topography and hydrological systems of glaciers. This paper determines for the first time how these influences impact on bulk water routing and the proglacial runoff signal, using analyses of supraglacial and proglacial water chemistry and proglacial discharge at Miage Glacier, Italian Alps. Debris does influence the supraglacial water chemistry, but the inefficient subglacial system beneath the debris-covered zone also plays a role in increasing the ion contribution to the proglacial stream. Daily hydrographs had a lower amplitude and later discharge peak compared to clean glaciers and fewer diurnal hydrographs were found compared to similar analysis for Haut Glacier d'Arolla. We attribute these observations to the attenuating effect of the debris on ablation,

smaller input streams on the debris-covered area, a less efficient subglacial system, and possible leakage into a raised sediment bed beneath the glacier. Strongly diurnal hydrographs are constrained to periods with warmer than average conditions. 'Average' weather conditions result in a hydrograph with reverse asymmetry. Conductivity and discharge commonly show anti-clockwise hysteresis, suggesting the more dilute, rapidly-routed melt component from the mid-glacier peaks before the discharge peak, with components from higher up-glacier and the debris-covered areas arriving later at the proglacial stream. The results of this study could lead to a greater understanding of the hydrological structure of other debris-covered glaciers, with findings highlighting the need to include the influence of the debris cover within future models of debris-covered glacier runoff.

1 Introduction

Glacial melt is an important component of downstream runoff, especially during dry seasons (Maurya et al., 2011; Xu et al., 2009). Understanding the runoff hydrograph is important for water resources management, for example for irrigation (e.g. in the Tien Shan region of China (Wang et al., 2014)); and the development of hydropower projects (e.g. in the Indian Himalaya (Srivastava et al., 2014)). There is a need to provide a more complete assessment of how glacier retreat may impact on hydropower revenues (Milner et al., 2017). The diurnal amplitude of runoff from clean glaciers is expected to increase and the lag time to peak runoff to decrease in a warmer climate as the snowpack has a progressively smaller hydrological influence (Escher-Vetter and Reinwarth, 1994).

However, given the likely increase in debris cover on alpine glaciers (Stokes et al., 2007), and the widespread occurrence of debris-covered glaciers in high-mountain regions (Scherler et al., 2018), projections of runoff hydrographs need to include debris cover effects. Debris-

covered glaciers are especially common in the Pamirs and Himalaya (Bolch et al., 2012; Scherler et al., 2011), Caucasus Mountains, Russia (Stokes et al., 2007) and the Western Alps (Deline et al., 2012) with the extent and thickness of debris cover increasing in many areas (Bhambri et al., 2011; Bolch et al., 2008; Kirkbride and Deline, 2013; Lambrecht et al., 2011). Supraglacial debris cover reduces melt compared to bare ice, except where the cover is thin or discontinuous (Kirkbride and Dugmore, 2003; Mattson et al., 1993; Østrem, 1959). Debris also reduces the amplitude of the melt signal and causes an increase in the lag from peak air temperature to peak melt, with the effect greater for thicker covers (Fyffe et al., 2014).

Recent dye tracing work (Fyffe et al., 2019) found that a supraglacial debris cover reduced meltwater inputs and resulted in less efficient flow beneath the debris-covered area. In contrast, up-glacier, the higher ablation rates of the clean and dirty ice and the focussing of supraglacial streams between moraine ridges produced an efficient conduit drainage system. Despite this new understanding, dye tracing can only ever elucidate the system efficiency for specific drainage routes during the time of the test, and cannot identify the proportion of water in each part of the system and how this varies diurnally and seasonally.

However, hydrochemistry and proglacial hydrograph investigations can reveal variations in bulk water routing, providing a complementary perspective on this rarely studied system. Glacier hydrochemistry can elucidate the conditions through which meltwater travels before emerging at the snout (see Brown (2002) for a review), with the glacial runoff pattern a function of the recharge (input) hydrograph and how it has been influenced by the glacier hydrological system (Covington et al., 2012). Essentially, the proglacial discharge and its chemistry provides a cumulative insight into all of the meltwater sources and their transport paths, so that if the chemical signature of a flow component (usually defined by a meltwater

source or transport path) is known, then its lag time and proportion of discharge can be determined (Brown, 2002). Understanding bulk water routing also allows a clearer understanding of the processes leading to sediment transport and solute acquisition. Variations in suspended sediment have implications for nutrient cycling (Hawkings et al., 2016; Hodson et al., 2004), and also influence turbidity, affecting light penetration and primary productivity (Milner et al., 2017).

Furthermore, there is currently little knowledge of how the unusual hydrological system identified from dye tracing affects the glacier hydrochemistry and proglacial runoff. Some work has dealt with solute, SSC and discharge characteristics of debris-covered glaciers (see Table 1), but these studies do not relate their findings to the existence of a supraglacial debris cover. We hypothesis that proglacial solute will be enhanced due to prolonged contact with debris both supraglacially and subglacially, especially for the delayed flow component composed of sub-debris melt. It is expected that the proglacial hydrograph will be relatively subdued, with a long time to peak discharge and a less strongly peaked diurnal hydrograph, given the known lag time to peak melt beneath debris (Fyffe et al., 2014), and the less efficient hydrological system beneath the lower glacier (Fyffe et al., 2019).

Using data collected from the debris-covered Miage Glacier, Italy, this paper therefore has the following aims:

1. Determine the influence of supraglacial debris on supraglacial and proglacial water chemistry.
2. Determine how the debris' impact on the supraglacial hydrograph and englacial and subglacial drainage system structure determine the form and magnitude of the proglacial hydrograph.

3. Establish an understanding of the main flow components in debris-covered glacier runoff.

2 Study Site

Miage Glacier is a 10.5 km^2 glacier with an elevation range of 1740 to 4640 m a.s.l., situated in the western Italian Alps (Figure 1). It sits within a catchment of approximately 22.7 km^2, bounded by the ridge crest from Pointe Baretti around to Petit Mont Blanc (Deline, 2005), and by large lateral moraines surrounding the lower glacier. Miage Glacier has four steep icefall tributaries: the Mont Blanc, Dome, Bionassay and Tête Carrée Glaciers. The main tongue occupies a deep trough from which it flows into Val Veny, bending eastwards and dividing into the large northern and southern lobes and a smaller central lobe. The glacier has a variety of surface types: at high altitudes clean ice and snow dominate; in the mid-part of the glacier (c. 2400-2600 m a.s.l.) relief is controlled by medial and lateral moraines, with a patchy covering of debris (hereafter 'dirty ice') in the intervening troughs; whereas the lower 5 km of the glacier is almost continuously covered by debris with a mean thickness of 0.25 m (Foster et al., 2012). The described extent of the continuous debris cover (relevant to the 2010/2011 field seasons) has existed since the 1930s (Deline, 2005), though there has been an observed increase in debris cover at the expense of the moraine-trough dirty ice since at least 2012. The debris originates predominantly from rockfalls and mixed snow and rock avalanches from the steep valley sides (Deline, 2009).

3 Methodology

Meteorological, hydrological and water chemistry measurements were conducted on Miage Glacier over the 2010 and 2011 summer seasons (Table 2).

3.1 Meteorology and melt modelling

Two energy balance weather stations were installed on continuous debris on the upper (UWS) and lower (LWS) glacier in 2010 and 2011, with a further station (IWS) measuring only air temperature situated over an area of thin and patchy debris in 2011 (Figure 1). For full details of the instrumentation and variables measured see Brock et al. (2010) and Fyffe et al. (2014).

A distributed energy balance melt model was constructed for Miage Glacier (see Fyffe et al. (2014) for detailed model methods and results). The model runs at an hourly timestep over a 30 x 30 m grid over the Miage Glacier catchment, with exactly the same inputs and parameters as outlined in Fyffe et al. (2014). The difference between simulated and measured melt at long term stakes was -0.001 m d^{-1} (5%), with the RMSE between simulated and measured debris surface temperature at LWS 1.8°C (R^2 = 0.95). Comparison between simulated melt plus effective precipitation (defined as rainfall minus evaporation, with rainfall distributed using a rainfall lapse rate derived from measured rainfall at tipping bucket rain gauges situated at LWS and UWS) and measured discharge resulted in a RMSE of 3.26 $m^3 s^{-1}$ in 2010 and 3.77 $m^3 s^{-1}$ in 2011, with a model bias of -0.94 in 2010 and -2.60 in 2011. This underestimation of discharge is likely due to raingauge undercatch since values corresponded well during dry periods. Note that no routing routines were applied to account for water transport through the hydrological system.

3.2 Supraglacial and proglacial water chemistry

Water samples were taken in the morning and afternoon at the gauging station during field visits, almost daily in June 2010 and every second or third day during other field trips. The average time of morning measurements in 2010 was 10:44 and in 2011 was 10:06, with the

137 average time of afternoon measurements 16:54 in 2010 and 16:43 in 2011. Conductivity and
138 water temperature were measured continuously at the gauging station (see Table 3) at one
139 minute intervals during field visits, and 30 minute intervals between visits. Unfortunately,
140 clogging of the probe with sediment resulted in large periods of erroneous conductivity data.
141 Conductivity data were collected from 23/06/2010 to 28/06/2010, from 28/07/2010 to
142 23/08/2010, from 06/09/2010 to 12/09/2010, from 05/06/2011 to 26/06/2011, from
143 26/07/2011 to 24/08/2011, and from 12/09/2011 to 15/09/2011, although there are smaller
144 gaps within these periods. Water samples were also collected from supraglacial streams,
145 ponds and lakes and three snow samples were melted and analysed, see Figure 1 and Table 4.
146 Sample locations were chosen to represent the range of supraglacial environments on the
147 glacier and allow the conditions conducive to solute and sediment acquisition to be
148 determined.

149 Water samples were filtered in the field using a Nalgene field filter holder and receiver and
150 hand pump, and a pre-weighed Whatman cellulose nitrate membrane filter (0.45 μm pore size
151 and 47 mm diameter), following standard procedures (Hubbard and Glasser, 2005). The filter
152 papers were oven dried and weighed in the laboratory to determine the suspended sediment
153 concentration (SSC). Each sample was stored in an acid-rinsed bottle in a cool bag or fridge
154 except during transit to the UK. Whenever a water sample was taken the conductivity, water
155 temperature, turbidity and pH of the stream, pond or lake was also measured using hand-held
156 probes (Table 3).

157 Each sample was tested for the concentration of sulphate and bicarbonate ions. These ions
158 were chosen due to their common use as indicators of the subglacial environment: sulphate
159 ions are generated by sulphide oxidation, within water routed slowly within a distributed
160 system (although snow and groundwater can also be a source of sulphate); with bicarbonate

ions generated from acid hydrolysis, signifying contact of meltwater with sediment either at the bed or suspended in-stream (Brown, 2002; Brown et al., 1996; Raiswell, 1984; Tranter et al., 1996; Tranter et al., 1993a; Tranter and Raiswell, 1991). Sulphate concentration was found by adding a powdered sulphate reagent, with the sample absorbance tested in a CECIL CE 4002 spectrophotometer (accuracy of ± 0.005A or 1%, whichever is greater). The test has a stated measurement range of between 2 and 100 mg l^{-1}. The measured absorbance was calibrated to sulphate concentration using a calibration curve. The results were not accepted if they differed by more than 100 µeq l^{-1}. For the remaining samples the mean (median) absolute difference between samples was 28.7 (19.4) µeq l^{-1} or 18 (12)% in 2010 and 9.3 (5.3) µeq l^{-1} or 51 (8)% in 2011. The mean percentage difference is larger in 2011 due to the increased number of lower concentration supraglacial samples.

The concentration of bicarbonate was found by titrating 20 ml of sample with 0.01 mol l^{-1} hydrochloric acid using Kittiwake pH 4.5 indicator. Two titrations were carried out on each sample, and they were accepted if the volume of hydrochloric acid added agreed within 2 ml (59.8 µeq l^{-1} of bicarbonate). If not then a third test was performed, and if two of the three tests agreed then their values were used instead. The average absolute difference between the tests was 24.7 µeq l^{-1} of bicarbonate (5%). Once both the sulphate and bicarbonate concentrations had been found they were used to calculate the C-ratio [$HCO_3^-/(HCO_3^- + SO_4^{2-})$] (Brown et al., 1996). The partial pressure of CO_2 was also calculated from the pH and bicarbonate concentration (see Brown (2002, equation 9)).

3.3 The impact of debris on the proglacial hydrograph

3.3.1 Field measurements

Proglacial runoff was derived from water level measurements and a rating curve collected at a gauging station located on the northern lobe stream, upstream of any confluences (GS in Figure 1). It consisted of a pressure transducer hung in a stilling well, bolted onto a very large boulder (see Table 3). The Onset HOBO pressure data were compensated using air pressure data from Mont de la Saxe, 7.6 km from the gauging station. Dye tracing indicates that the small outflow from the southern lobe is derived locally from only the area of that lobe (Fyffe, 2012) so the runoff from the rest of the glacier exits via the northern lobe. A high flow event in June 2011 caused damage to the well, resulting in data loss between 18/06/2011 and 03/08/2011 and the repositioning of the well. Data was also lost between 27/08/2010 and 28/08/2010 and between 04/09/2010 and 08/09/2010. The measured stages from all time periods were adjusted to the datum of the June 2010 well so that one stage-discharge rating could be applied. A total of 16 rhodamine WT dye-dilution gaugings were used to construct a two-part rating curve with a percentage error of 14.6% (see Supplementary Information A for further details).

3.3.2 Analysis of the proglacial runoff record

Daily hydrographs were categorised into shape categories following Hannah et al. (2000, 1999) and Swift et al. (2005). The hydrograph classes were predetermined and hydrographs classified manually to allow a more direct comparison of results with other workers. The runoff record was divided into 24 hour periods (‘days’) with the beginning of the ‘day’ being the average time of minimum runoff (for complete days with no rain) of 11:00 in 2010. Daily hydrographs were classified as either:

i. diurnal (a peak in the middle of the day, and lower flows at the beginning and end)
ii. rising,
iii. falling, or
iv. unknown (hydrograph steady or could not be assigned to one of the other categories).

If a hydrograph fell between two categories then the most prominent feature of the hydrograph was used to determine its category. Only complete days with no rain were categorised. Mean hydrographs for categories i) to iii) are in Figure 2. Following Swift et al. (2005) specific parameters were calculated for each of the hydrographs classified as diurnal, as well as averages for each year, see Table 5.

The 2010 and 2011 melt season hydrographs were delimited into phases based on the dominant hydrograph type (Figure 3). The percentage of days of each hydrograph type (diurnal, rising or falling, not including unknown hydrographs) was calculated for a running 10 day period, with the mid-day of the 10 day period used as the phase boundary. The early season period is phase 1. Later in the season (from the beginning of July onwards) hydrographs are classified as either Phase 2, when more than 50% of the hydrographs are diurnally-classified, or Phase 3, when less than 50% of the hydrographs are diurnally-classified.

To find the lag time between peak air temperature and discharge, the time between maximum air temperature and maximum discharge was calculated (with the day starting at 11:00). Lag times were also calculated between maximum air temperature and minimum conductivity and between minimum conductivity and maximum discharge. Only diurnally-classified conductivity data (defined as having a minimum conductivity in the middle of the day and higher values before and after this) were used in this analysis. Lag times were also calculated

statistically using a lag correlation between hourly discharge and air temperature records from LWS and UWS. The discharge record was moved back in time in hourly increments and the correlation repeated up to a lag of 24 hours, with the lag time with the highest correlation coefficient giving the average lag time. The records were also split into 10 day periods and the process repeated, to reveal seasonal changes. Only the 2010 record was used in the statistical analysis, due to its completeness, and all days were included.

4 Results

4.1 The influence of debris on supraglacial and proglacial water chemistry

4.1.1 Supraglacial water chemistry

Supraglacial water chemistry results are given in Table 4, with sulphate and bicarbonate concentrations shown in Figure 4. There is a distinction in bicarbonate concentrations between the two largest streams on the upper glacier (S12 and S14) which demonstrated lower bicarbonate concentrations (and also lower SSC), and most of the other samples which had bicarbonate concentrations around 300 µeq l^{-1}. Note that although S15 was close to S12 and S15 it had a smaller, mainly debris-covered catchment. SP5 (a small pond) had the highest bicarbonate concentrations, with the lower glacier streams S1 and S7 also showing elevated concentrations. The average supraglacial stream bicarbonate concentration was much lower (286 µeq l^{-1}) than the proglacial stream values (783 µeq l^{-1} in 2010 and 603 µeq l^{-1} in 2011).

There was not a distinction in sulphate concentrations between the larger upglacier streams and the smaller streams on the lower glacier. However, the sulphate concentration of SP5 was particularly high (87 µeq l^{-1}), with the values for the C4 and C8 lakes also high compared to

the supraglacial streams. The elevated sulphate concentrations measured at WS5 are likely because the samples were taken in early June 2010 when its catchment was snow-covered, since snow sample 3 demonstrated elevated sulphate concentrations. The mean sulphate concentration of supraglacial stream measurements of 16 μeq l^{-1} was an order of magnitude lower than gauging station values.

4.1.2 Proglacial water chemistry

The concentration of sulphate ions measured at the proglacial stream was high compared with other clean glaciers (Table 6), with values most similar to the debris-covered Dokriani Glacier outside of the monsoon season. The highest values of sulphate on Miage Glacier were either when there was a pulse of ion and sediment rich water (09/06/2010, 474 μeq l^{-1}, corresponding to a fall in discharge and a peak in conductivity, SSC and bicarbonate concentration) or when discharges were low during cold weather (e.g. 367 μeq l^{-1} on 20/06/2010 and 383 μeq l^{-1} on 15/09/2011). Even though the highest sulphate concentration measured was on 09/06/10, the delayed-flow sulphate concentrations were still high even in mid-summer (Table 4). The variation between different times of year was small with the difference between mean June, and mean July/August concentrations being only 5 μeq l^{-1} in 2010, and 25 μeq l^{-1} in 2011. This contrasts with Haut Glacier d'Arolla and Austre Brøggerbreen where June sulphate concentrations were at least twice those later in the season (Tranter et al., 1996). The relationship between sulphate and discharge was generally weak, so in 2010 the only relationship with discharge was in September when the sulphate concentration increased as discharge decreased (p-value 0.016, R^2 = 37.3), although in 2011 this negative relationship was also found in June (p-value 0.009, R^2 = 27.4), and more strongly in July and August (p-value 0.017, R^2 = 58.4).

Even taking account of the elevated supraglacial bicarbonate concentrations (section 4.1), the mean and range of proglacial values are still high compared to clean glaciers (Table 6). The values are most similar to the debris-covered Batura Glacier and Dokriani Glacier during the monsoon season, slightly above the values for Grimsvötn, and below those from the icing at Scott Turnerbreen. As for sulphate, bicarbonate concentrations were highest either in June 2010 when there was a pulse of sediment and ion rich water (913 μeq l^{-1} on 09/06/2010 at 10:05), or during recessional flow, for instance 1092 μeq l^{-1} at 10:30 on 22/06/2010, corresponding with a particularly low discharge of 1.65 m^3 s^{-1}. The bicarbonate concentration decreased over the season in 2010, but this was not mirrored in 2011. Unlike sulphate, the bicarbonate concentration never had a significant relationship with discharge in 2010 or 2011.

4.2 The impact of debris on the proglacial hydrograph

The runoff and meteorological conditions in 2010 and 2011 are given in Figure 5. Average values are calculated for the melt season, with 2011 meteorological averages found for the same dates as the 2010 record (see Table 2).

4.2.1 Hydrograph shape classification

Hydrograph shape classification (Table 7) revealed that the majority of hydrographs were diurnal in both years, with almost as many rising but fewer falling hydrographs. Of the diurnally classified hydrographs in 2010 (2011), 7 (6) were found in June, 14 (no data) in July, 8 (16) in August and 3 (3) in September. Even diurnally classified hydrographs often did not smoothly rise or fall and could exhibit a flattened or variable peak. Hannah et al. (2000) and Swift et al. (2005) classified daily hydrographs from Haut Glacier d'Arolla into shape categories, with Hannah et al. (1999) conducting similar analysis on Taillon Glacier

runoff. The Haut Glacier d'Arolla and Taillon Glacier runoff records were classified using principle component analysis, meaning the hydrograph classes were statistically derived and unique to the runoff record. A direct comparison with the Miage Glacier classes (although predetermined and conducted manually to aid comparison) should therefore be treated with caution. Nevertheless, Table 7 shows Miage Glacier has fewer diurnal hydrographs over the season than was classified for Haut Glacier d'Arolla in 1998 and 1999. Miage Glacier had a similar number of diurnal hydrographs to Taillon Glacier (and Haut Glacier d'Arolla in 1989), but some of the 'Building/Late peaked' hydrographs (which rise to a peak around 24:00) would have been classed as diurnal for Miage Glacier.

4.2.2 The amplitude of diurnal hydrographs

The diurnal runoff amplitude, described by Q_{dmax}/Q_{dmin}, can be compared to other clean and debris-covered glaciers (Tables 8 and 9). The range for Miage Glacier (from 1.2 in June/phase 1, to 2.12 in phase 3a) is similar to Dokriani Glacier, slightly higher than Gangotri Glacier and always higher than Dunagiri Glacier. The aforementioned glaciers are all debris-covered and their values (including those of Miage Glacier) are all lower than those given for the clean Qiyi and Parlung No. 4. Glaciers. Although the glacier area may alter the discharge ratio, the glacier area of Miage Glacier and Parlung No. 4 are very similar (Table 10). Values of Q_{dsdamp} found by averaging values for peaked hydrographs of different magnitudes were also given by Swift et al. (2005) for Haut Glacier d'Arolla. The Swift et al. (2005) values ranged from 0.83 to 2.40 (equating to Q_{dmax}/Q_{dmin} of 1.83 to 3.40), which appears relatively high compared to values for both Miage Glacier and the other debris-covered glaciers. Similarly found values of Q_{dsdamp} given by Hannah et al. (1999) for Taillon Glacier ranged from 0.434 to 2.649 (equating to Q_{dmax}/Q_{dmin} of 1.434 to 3.649), again giving high values

compared to the debris-covered glaciers. This suggests that the diurnal runoff amplitude of debris-covered glaciers is less than clean glaciers.

4.2.3 Lag time analysis

Lag times between air temperature and peak discharge determined by analysis of daily hydrographs are shown in Table 11. The mean and minimum lag times of the debris-covered glaciers are greater than that of the clean glaciers. The maximum lag time was greatest for Parlung No. 4 Glacier, but this value could have been influenced by colder weather in October. Lag times were also derived by conducting lag correlations between discharge and air temperature in 2010. All correlations were statistically significant ($p < 0.05$), with correlations generally stronger with UWS than LWS. The lag time for the whole discharge time series was between 9 and 10 hours (UWS relationship). Table 12 compares statistically derived lag times for a range of glaciers. The two debris-covered glaciers (Miage Glacier and Keqikaer Glacier) have longer minimum lag times than all of the clean glaciers. Baounet Glacier and Haut Glacier d'Arolla are both temperate alpine glaciers, similar to Miage Glacier, and both their maximum and minimum lag times are much lower than the values for Miage Glacier (by 14-15 hours and 4-7 hours, respectively). Despite the small data set there is therefore evidence that there is a greater lag time between peak air temperature and peak runoff for the debris-covered glaciers compared to the clean glaciers.

Lag times from peak air temperature to minimum conductivity (3.47 and 2.75 hours in 2010 and 2011 respectively) were shorter than between peak air temperature and peak runoff (6.34 and 7.92 hours in 2010 and 2011 respectively). When both diurnally classified proglacial discharge and diurnally classified conductivity data were available (only 8 days in total, see Figure 6) there was often a delay between the time of lowest conductivity and highest

discharge, resulting in discharge and conductivity rising in phase for a few hours. The mean time between minimum conductivity and maximum discharge in 2010 (2011) was 2.5 (4.25) hours.

Figure 6 shows the temporal change in the relationship between conductivity and discharge on individual days. The clearest cyclic hysteresis is anticlockwise, resulting in conductivity increasing with discharge in the evening (or sometimes high but variable discharge and increasing conductivity). For conductivity to increase with discharge, the solute load must be increasing at a greater rate than discharge (Fountain, 1992).

4.2.4 Runoff fluctuations and their relation to meteorological variations

Phase 1: Early season runoff

During the entire phase 1 period in 2010 and prior to 13/06/11 in the 2011 record discharges generally remained low (average 3.2 $m^3 s^{-1}$ and 2.1 $m^3 s^{-1}$ for 2010 and 2011 respectively), and although diurnal hydrographs dominated they had a small amplitude. In 2010 variations over a few days had a larger magnitude than diurnal fluctuations. In 2011 discharges rose on 13/06/11 but did not rise substantially until 15/06/11, followed by the large flood event on 18/06/11 caused by very heavy rainfall (Figure 5). In both years air temperatures during Phase 1 periods were lower than average.

Phase 2: Diurnal runoff

During phase 2 in both years the discharge increased, alongside an increase in the percentage of diurnal hydrographs and the mean amplitude of diurnal hydrographs (to 5.0 $m^3 s^{-1}$ in both years) (Figure 7a and b). These changes were driven by consistently fine weather with increased air temperatures and only occasional rainfall (mean LWS air temperature in Phase

363 2 was greater than average by 4.4°C in 2010 and 2.3°C in 2011). The flows in 2010 did not
364 increase until around three days after the rise in air temperature, although within the phase 2
365 period the discharge was more responsive to meteorological changes (e.g. the shape of the
366 hydrograph peak relates to the hourly modelled ablation on 11/07/10, see Figure 7a).

367 **Phase 3: Hydrographs with reverse asymmetry**

368 The phase 3 runoff in 2010 begins around 16/07/10 (Figure 7c). The overall discharge
369 magnitude was similar to average (5.9 $m^3 s^{-1}$, average 5.3 $m^3 s^{-1}$), with the discharge
370 amplitude larger than average (2.7 $m^3 s^{-1}$ for diurnal hydrographs only, with 3.4 $m^3 s^{-1}$ the
371 average). The lag time to peak discharge for diurnal hydrographs (4.46 hours) was shorter
372 than average and for phase 2, but including all hydrographs was much longer (8.17 hours).
373 The mean air temperature at LWS was within 1°C of the average.

374 The phase 3 runoff in 2011 occurred both before (phase 3a) and after (phase 3b, Figure 7d),
375 the phase 2 runoff period. The mean discharge of the phase 3a and 3b runoff for diurnal and
376 all hydrographs was higher (3a) and lower (3b) than average but by not much more than 1 m^3
377 s^{-1}. The discharge amplitude was higher than average (using only diurnal hydrographs) in
378 phase 3a but lower than average in phase 3b. Using both diurnal and all hydrographs the lag
379 time of phase 3a and 3b (around 9-10 hours) was higher than phase 2 and the seasonal
380 average. The mean air temperature at LWS of the phase 3a and 3b periods was also within
381 1°C of the average.

382 Phase 3 runoff tends to show reverse asymmetry in 2010 and 2011 (see Figure 7c). The
383 increasingly warm air temperatures between 30/07/10 and 01/08/10 lead to a gradually rising
384 hydrograph, then after the precipitation inputs passed and the weather cooled the runoff
385 decreases. Warmer temperatures lead to gradually increasing discharges, but a decrease in air

386 temperature leads to a sharp runoff decrease. In 2011, Figure 7d shows the rise in night-time
387 air temperature on 28/08/10 results in a rising hydrograph on 29/08/10. In the following days
388 the discharge does become diurnal but the minimum flow has a clearer trough than the
389 maximum flow has a peak.

390 # 5 Discussion

391 ## 5.1 The influence of debris on supraglacial and proglacial water chemistry

392 The proglacial concentration of sulphate and bicarbonate ions was high for Miage Glacier
393 compared with clean glaciers (section 4.1.2). The concentration of sulphate ions can be
394 influenced by a) snowpack sulphate derived from deposition of mainly the sea salt aerosol
395 (Tranter et al., 1996); b) contact of water with sediment at the bed resulting in sulphide
396 oxidation (Tranter et al., 1993b); or c) by the influence of groundwater. The influence of
397 supraglacial debris on sulphate concentrations is not known from previous studies.

398 Sulphate values in snow were low, with a mean concentration of 76 µeq l^{-1}, compared to 215
399 µeq l^{-1} on average in the proglacial stream in 2011 (Table 4). Most supraglacial streams had
400 very low sulphate concentrations, demonstrating that they mainly contained ice melt. There
401 was not a clear distinction in sulphate concentrations between the upper and lower glacier
402 supraglacial stream samples, suggesting that supraglacial debris does not increase the
403 sulphate concentrations. However, a higher sulphate concentration was measured in the small
404 pond SP5, suggesting that the longer sediment contact was conducive to coupled sulphide
405 oxidation and carbonate dissolution reactions which produce bicarbonate and sulphate ions
406 (Brown, 2002). However, the small ponds were not prevalent enough to be a significant ion
407 source. Similar conditions likely occur in the larger lakes (C4 and C8), although meltwater
408 from their large ice cliffs would lower ion concentrations. The lake ion concentrations were

lower than proglacial values, with lakes only providing ions to proglacial runoff upon drainage. Therefore, apart from the early season snowmelt, most proglacial sulphate is not of a supraglacial origin.

The lower glacier streams draining debris-covered catchments had higher bicarbonate concentrations than the upper streams draining mainly clean ice. Contact of meltwater with debris (possibly while within the debris matrix) therefore results in enough water-rock interaction to enrich the bicarbonate concentration through acid hydrolysis. The greater sediment availability may also lead to a higher SSC, allowing in-stream acid hydrolysis and the production of bicarbonate ions, even in ice-walled streams (Tranter et al., 1993a). Ice cliff meltwater may reduce bicarbonate concentrations (e.g. at S5 which is a stream bounded by ice cliffs in a thickly debris-covered catchment). Concentrations were higher in SP5, again suggesting that small ponds may be an ion source. Although debris enriched the supraglacial bicarbonate concentration, the average supraglacial stream concentration (286 $\mu eq\ l^{-1}$) was still considerably lower than the average gauging station concentration (783 $\mu eq\ l^{-1}$ in 2010 and 603 $\mu eq\ l^{-1}$ in 2011). Given the difference in supraglacial and proglacial concentrations of both bicarbonate and sulphate concentrations there must therefore be a significant proportion of the proglacial concentration produced instream, from groundwater, or at the bed.

It is most likely that the proglacial ions are produced from reactions within a distributed hydrological system which underlies the lower glacier, since there is already evidence of its existence from dye tracing (Fyffe et al., 2019). The ions could also be produced if water spent time in the sedimentary raised bed underlying the lower glacier (Pavan et al., 1999, cited in Deline, 2002). Both of these environments would contain freshly comminuted rock flour and be conducive to long enough residence times to elevate sulphate concentrations (Tranter et al., 1993b; Tranter and Raiswell, 1991). Both bicarbonate and sulphate concentrations

433 remained high throughout the melt season, suggesting that a significant proportion of
434 meltwater passed through the distributed system even in mid-summer (section 4.1.2).

435 Groundwater was sampled from a spring next to the valley river, the Dora d'Veny (Figure 1)
436 and concentrations of sulphate and bicarbonate were very high (2959 μeq l^{-1} and 1361 μeq l^{-1},
437 respectively), with a C-ratio of 0.32. However, the C-ratio was much lower than the lowest
438 value measured at the proglacial stream (0.63). Even if the bicarbonate concentration is
439 artificially increased by 286 μeq l^{-1} to account for the average supraglacial input of
440 bicarbonate ions, the C-ratio is still 0.36. The sulphate concentrations were twice the highest
441 values found from boreholes beneath Haut Glacier d'Arolla, with such high values suggesting
442 long residence times in anoxic conditions, where sulphide oxidation may be catalysed by
443 microbial activity (Brown, 2002). It is therefore less likely the proglacial ions are derived
444 from groundwater (at least that of a composition similar to the spring measured).

445 Furthermore, although bicarbonate ions can be produced within post-mixing chemical
446 reactions (Tranter et al., 1993a), the bicarbonate and sulphate ion concentrations tend to vary
447 together (although the only significant relationship was in July/August 2010). They also tend
448 to be high during low flow periods, suggesting that a portion of the bicarbonate concentration
449 is produced subglacially.

450 **5.2 The impact of debris on the proglacial hydrograph**

451 *5.2.1 The influence of supraglacial debris on proglacial discharge amplitude and lag time*

452 Comparison of the lag time and diurnal discharge amplitude of debris-free and debris-covered
453 glaciers (sections 4.2.2 and 4.2.3) suggests that glaciers with an extensive supraglacial debris
454 cover have a more subdued proglacial hydrograph with a smaller amplitude and longer lag

time between peak air temperature and discharge compared to clean glaciers. This corroborates the findings of Li et al. (2016) in the Tibetan Plateau and corresponds with the lower overall percentage of diurnal hydrographs found when comparing Miage Glacier and Haut Glacier d'Arolla (section 4.2.1). However, comparable data were only available for 6 debris-covered and 6 clean glaciers for lag time analysis and 4 debris-covered and 4 clean glaciers for diurnal discharge amplitude parameters.

The lower discharge amplitude and fewer diurnal hydrographs under average weather conditions could be due to a more subdued input (or recharge) hydrograph (Covington et al., 2012). An attenuated input hydrograph from debris-covered areas will be caused by the time taken for the temperature signal to be conducted down through the debris to the ice-debris interface, resulting in melt continuing into the evening (Fyffe et al., 2014 (especially Figure 7); Nicholson & Benn, 2006; Reid & Brock, 2010). This increases the lag time between peak air temperature and peak melt, which increases with increasing debris thickness (although the runoff delay will be less than that of the average debris thickness since more melt is produced beneath thinner debris) (Fyffe et al., 2014). Thus, supraglacial debris will reduce the amplitude of the input hydrograph, increasing the baseflow and decreasing the diurnal discharge amplitude.

Furthermore, melt must flow within the debris and/or at the ice/debris interface prior to reaching a supraglacial stream. Flow velocities in this system are unknown but it may provide a further delay to water transfer. Flow within streams within the debris-covered region of Miage Glacier is known to be relatively slow (Fyffe et al., 2019) and Miles et al. (2019) reported slow flow velocities between an interconnected pond system on Khumbu Glacier. The relatively inefficient supraglacial transfer of meltwater within the debris-covered region

would increase the time between melt production and input into the englacial/subglacial system.

The input hydrograph could also be attenuated by an inefficient englacial or subglacial system, or the existence of a subglacial aquifer (Flowers, 2008; Flowers and Clarke, 2002). An inefficient englacial/subglacial system was found beneath the debris-covered area (Fyffe et al., 2019), with the high proglacial bicarbonate and sulphate concentrations further confirming its existence (section 5.1). The volume of storage is key to determining whether or not recharge hydrographs are altered by the glacial drainage system (Covington et al., 2012). Flowers (2008) identified that a subglacial aquifer can attenuate hydrographs, and while Covington et al. (2012) demonstrated that although conduits and a linked cavity system did not normally modify the recharge hydrograph, they could if linked to sufficiently large storage such as crevasses or lakes. The inefficient englacial/subglacial system could therefore alter the recharge hydrograph if the degree of storage in the system was sufficient.

The thickness and hydraulic conductivity of the bed materials could also have a significant influence on the discharge amplitude and lag time (Flowers, 2008; Flowers and Clarke, 2002). The lower Miage Glacier sits on a sediment bed, around 50 m thick (Pavan et al. (1999) cited in Deline (2002)). Flowers (2008) showed that a ‘soft’ sediment bed would lower the amplitude of diurnal fluctuations, increasing the lag time from peak melt to peak discharge and inhibiting conduit formation, compared to a ‘hard’ bedded glacier. Flowers (2008) also showed that a subglacial aquifer beneath the sediment bed would further reduce the discharge amplitude, with the effect increasing with aquifer thickness and hydraulic conductivity. This is driven by higher water pressures resulting in flow being transferred from subglacial channels to be stored in the surrounding sediments, with water flowing back to the channels as pressures drop (Hubbard et al., 1995). Debris-covered glaciers often rest on

sedimentary beds, since a substantial supraglacial debris cover indicates a high rate of debris supply and high englacial debris concentrations (Maisch et al., 1999). Low sub-debris melt rates and a long, low angled tongue would likely also reduce the debris transport capability of meltwater streams, with debris accumulating at the bed as a result. The impacts of a raised-bed sediment aquifer on the proglacial hydrograph may therefore also apply to other debris-covered glaciers.

Whether the lag time from peak air temperature to peak discharge is increased due to the debris-cover for a particular glacier will depend upon the debris thickness distribution and its proportional cover over the glacier, since these factors will influence the proportion of sub-debris melt and the average delay due to conduction of heat to the ice-debris interface. If rapidly-routed clean ice melt is a large enough proportion of runoff, then the lag time may not be influenced by the debris cover since the clean ice component will provide the discharge peak (c.f. Miage Glacier in section 5.3). Furthermore, the bed composition (bedrock or sedimentary) and the thickness and hydraulic conductivity of any raised bed could influence the amplitude and timing of the proglacial hydrograph (Flowers, 2008; Flowers and Clarke, 2002).

5.2.2 Runoff fluctuations and their relationship to meteorological conditions

Phase 1 proglacial hydrographs were subdued in both years even though most of the lower glacier was snow free (from 2290 m a.s.l. in 2010 and 2400 m a.s.l. in 2011) and dye tracing suggested the main subglacial channel system was open and efficient (from at least 09/06/10 and 10/06/11 (Fyffe et al., 2019)). On the upper glacier the snow cover would have reduced the supraglacial hydrograph amplitude and increased the meltwater travel time (Campbell et al., 2006; Willis et al., 2002). Meanwhile, on the debris-covered lower glacier meltwater

inputs would be small and attenuated due to the conduction of heat through the debris (Fyffe et al., 2014), and smaller supraglacial streams (Fyffe et al., 2019). Meltwater from the debris-covered region will therefore have a subdued hydrograph, and if the stream passes through the distributed system underlying the lower glacier (see section 5.1 and Fyffe et al. (2019)) it may be delayed englacially and subglacially too. This means that a proglacial hydrograph with a smaller amplitude and longer lag from peak air temperature to peak discharge can result even if a large proportion of the lower glacier is snow-free, if the snow-free region is instead debris-covered.

Phase 2 periods were found during warmer than average weather conditions. By mid-summer large areas of clean and dirty ice were snow-free, with the snowline up to approximately the base of the Bionassay Glacier by 31/07/10 and slightly less coverage in 2011. The removal of snowcover from the debris-free area would have increased the magnitude and amplitude of meltwater inputs to the upper glacier moulins (e.g. S12 and S14) (Willis et al., 2002). The main subglacial drainage system remained efficient in both years, and although the drainage system beneath the debris-covered area increased in efficiency, it was still less efficient than that emanating from higher on the glacier (Fyffe et al., 2019). Continued drainage through the distributed system is also confirmed by the proglacial sulphate and bicarbonate concentrations which remained high throughout the summer (section 5.1). Removal of snow from the clean and dirty ice area is therefore required to increase the amplitude of the upglacier supraglacial hydrograph and therefore lead to a clear proglacial diurnal signal. Phase 2 periods therefore require consistently warm and dry weather as well as the loss of snow cover from the upglacier clean ice.

Phase 3 runoff occurred during average weather conditions, and resulted in close to average proglacial discharges and diurnal amplitudes and a hydrograph with reverse asymmetry

where flow increases gradually but falls quickly. Smeared or multiple hydrograph peaks could be caused by multiple input points with different lag times (Covington et al., 2012). Since variations in debris thickness cause variations in the time of the supraglacial hydrograph peak (Fyffe et al., 2014), and the debris morphology leads to many, smaller input points (Fyffe et al., 2019; Miles et al., 2017), this may result in a flattened peak, especially if cooler weather means a larger proportion of runoff is from the debris-covered area.

The reverse asymmetry of the phase 3 runoff hydrograph is somewhat unusual. A possible explanation involves percolation of meltwater into the sediment aquifer beneath the lower glacier. If the input of water into the subglacial system is less than the maximum potential rate of infiltration into the aquifer (which would depend upon the aquifer hydraulic conductivity), the aquifer could essentially capture the drainage (Flowers and Clarke, 2002). Net loss to the aquifer would be especially noticeable when most meltwater is introduced from further upglacier, and inputs from the lower glacier are limited.

A second possible mechanism involves the overdeepening which occurs just upstream of the bend in the main tongue (Pavan et al. (1999) cited in Deline (2002)). Water pressures close to overburden are required for subglacial water to flow up the adverse bed slope and exit the overdeepening. The rise in the pressure melting point as the water flows up the adverse bed slope can result in supercooling, forming frazil ice which can reduce the hydraulic conductivity and subsequently flow rates (Alley et al., 1998). Whether or not supercooling occurs is dependent upon the riegel slope angle (Alley et al., 1998), how close the water temperature is to the melting temperature, and by water pressure variations (Dow et al., 2014). If the riegel is steep enough, water flow could be restricted, especially when water pressures are lower (Dow et al., 2014), potentially increasing hydrograph recession.

5.3 The flow components of Miage Glacier runoff

By combining the results of the hydrochemistry (section 5.1) and proglacial discharge analysis (section 5.2) the main flow components of Miage Glacier runoff can be identified (Figure 8). Supraglacial hydrochemistry demonstrated that upper glacier clean ice melt does not tend to acquire solutes, with dye tracing revealing that upper glacier meltwater is drained efficiently (Fyffe et al., 2019). The fast transfer of this dilute clean ice melt component suggests its peak at the proglacial stream is indicated by the conductivity minimum which arrives around 3 hours after peak air temperature (section 4.2.4).

Meanwhile, on the debris-covered lower glacier, the small supraglacial streams flow more slowly (Fyffe et al., 2019), with meltwater acquiring bicarbonate ions due to its contact with sediment (section 4.1.1). Dye tracing indicated some of the lower glacier subglacial drainage pathways were inefficient (Fyffe et al., 2019), with the high proglacial sulphate and bicarbonate concentrations confirming this (section 5.1). Sub-debris melt will therefore likely have a greater solute concentration and take longer to arrive at the snout. This explains the evening rise of conductivity with discharge shown in Figure 6 – the delayed 'debris' component becomes a larger proportion of runoff in the evening and likely peaks when the discharge peaks 6-8 hours after peak air temperature. However since modelling suggested melt from the debris-covered region provided only 27-30% of total melt (Fyffe et al., 2014), melt from the tributary glaciers very high upglacier may constitute the remainder of the discharge peak. The longer travel times of the 'debris' component explains the observed long lag times between air temperature and peak discharge for debris-covered glaciers (section 4.2.3).

Presuming that the ‘clean ice’ component peaks at the time of minimum conductivity, while the ‘debris’ component peaks at the time of maximum discharge, then the overall delay due to the debris cover averaged over the glacier can be calculated from the difference between these times (2.5 hours in 2010 and 4.25 hours in 2011, based on 8 days of conductivity data). Several mechanisms could account for this delay (section 5.2.1), including attenuation of the melt signal due to conduction of heat through the debris, smaller supraglacial streams, a less efficient englacial/subglacial hydrological system and a sediment bed. The delay due to heat conduction averaged over the glacier is around 1-2 hours (Fyffe et al., 2014), with the less efficient englacial/subglacial system resulting in a delay of around 1.9 hours (Fyffe et al., 2019) (Supplementary Information B outlines how these delays were derived). Since these delays are roughly equal in duration both should be included in debris-covered glacier runoff models. Supraglacial dye tracing is needed to determine the supraglacial efficiency of debris-covered glaciers, while further runoff modelling would be needed to fully understand the influence of a sediment aquifer.

6 Conclusions

Supraglacial debris influences glacier hydrochemistry in two main ways. Firstly, greater supraglacial water-rock contact on the lower glacier increases the SSC and bicarbonate concentration of supraglacial lakes and streams. The supraglacial debris only influences sulphate concentrations where residence times are long (e.g. in small ponds). Secondly, since the debris cover inhibits the formation of a channelised network beneath thickly debris-covered areas (Fyffe et al., 2019), it indirectly increases the proglacial bicarbonate and sulphate concentrations by increasing the proportion of water which is routed through an inefficient subglacial system.

The Miage Glacier runoff hydrograph is a product of the melt signal and its alteration by the hydrological system. Since the supraglacial debris attenuates the melt signal (Fyffe et al., 2014) and results in an inefficient subglacial system fed by smaller input streams (Fyffe et al., 2019) this means the flow component composed of sub-debris melt has a longer lag time than the flow component from the clean and dirty ice which is routed efficiently from the mid-glacier. This increases the discharge baseflow and increases the lag time between peak air temperature and peak runoff, although the raised sediment bed may also play a role in attenuating the proglacial hydrograph. Discharge and conductivity commonly showed anti-clockwise hysteresis with conductivity and discharge rising in phase for a few hours. This suggests that the dilute melt component likely peaks before the more ion rich 'debris' and 'tributary' components. The delaying effect of the debris also means that both a snow-free upper glacier and particularly warm weather are required for diurnal hydrographs to dominate. Under average weather conditions rising or falling hydrographs dominate and the hydrograph tends to rise more slowly than it falls, resulting in reverse asymmetry in the hydrograph.

These conclusions show that the hydrochemistry and proglacial runoff signal of debris-covered glaciers differs from clean glaciers. Given that data for comparison was from a relatively small sample of glaciers, work to increase this sample size and differentiate the influence of specific catchment and debris characteristics on the proglacial runoff signal would be welcomed. These findings will be relevant to other catchments with debris-covered glaciers, and those that are likely to become more debris-covered in the future (e.g. Bhambri et al., 2011; Bolch et al., 2008; Lambrecht et al., 2011). Since receding glaciers may become more debris-covered, the influence of supraglacial debris on the runoff hydrograph should be accounted for within future runoff models. The present study is a pioneering first step towards quantifying the influence of debris and glacier characteristics on supraglacial and

proglacial hydrographs. It will inform future work involving the direct comparison of hydrographs from multiple glaciers using a consistent methodology and the construction of a physically-based hydrological model which takes into the account the influence of the debris on runoff. This would allow the prediction of runoff given changes to the debris cover.

7 Acknowledgements

This work was undertaken while C. Fyffe was in receipt of a studentship from the School of the Environment, University of Dundee. Air pressure data from Mont de la Saxe was kindly provided by F. Brunier from Regione Autonoma Valle d'Aosta. Students from the University of Dundee, Northumbria University, Aberdeen University and Cambridge University as well as L. Gilbert provided invaluable help in the field. M. Vagliasindi and J.P. Fosson of Fondazione Montagna Sicura provided excellent logistical support at the field site. The VDA DEM in Figure 1 was kindly provided by Regione Autonoma Valle d'Aosta (Modello Altimetrico Digitale della Regione Autonoma Valle d'Aosta aut. n. 1156 del 28.08.2007).

8 References

Alley, R.B., Lawson, D.E., Evenson, E.B., Strasser, J.C., Larson, G.J., 1998. Glaciohydraulic supercooling: a freeze-on mechanism to create stratified, debris-rich basal ice: II . Theory. J. Glaciol. 44, 563–569.

Anderson, S.P., Drever, J.I., Frost, C.D., Holden, P., 2000. Chemical weathering in the forefield of a retreating glacier. Geochim. Cosmochim. Acta 64, 1173–1189.

Bhambri, R., Bolch, T., Chaujar, R.K., Kulshreshtha, S.C., 2011. Glacier changes in the Garhwal Himalaya, India, from 1968 to 2006 based on remote sensing. J. Glaciol. 57, 543–556. https://doi.org/10.3189/002214311796905604

Bolch, T., Buchroithner, M., Pieczonka, T., Kunert, A., 2008. Planimetric and volumetric glacier changes in the Khumbu Himal, Nepal, since 1962 using Corona, Landsat TM and ASTER data. J. Glaciol. 54, 592–600. https://doi.org/10.3189/002214308786570782

Bolch, T., Kulkarni, A., Kääb, A., Huggel, C., Paul, F., Cogley, J.G., Frey, H., Kargel, J.S., Fujita, K., Scheel, M., Bajracharya, S., Stoffel, M., 2012. The State and Fate of Himalayan Glaciers. Science (80-.). 336, 310–314. https://doi.org/10.1126/science.1215828

Brock, B.W., Mihalcea, C., Kirkbride, M.P., Diolaiuti, G., Cutler, M.E.J., Smiraglia, C., 2010. Meteorology and surface energy fluxes in the 2005–2007 ablation seasons at the Miage debris-covered glacier, Mont Blanc Massif, Italian Alps. J. Geophys. Res. 115, D09106. https://doi.org/10.1029/2009JD013224

Brown, G.H., 2002. Glacier meltwater hydrochemistry. Appl. Geochemistry 17, 855–883. https://doi.org/10.1016/S0883-2927(01)00123-8

Brown, G.H., Sharp, M., Tranter, M., 1996. Subglacial chemical erosion: seasonal variations in solute provenance, Haut Glacier d'Arolla, Valais, Switzerland. Ann. Glaciol. 22, 25–31.

Campbell, F.M.A., Nienow, P.W., Purves, R.S., 2006. Role of the supraglacial snowpack in mediating meltwater delivery to the glacier system as inferred from dye tracer investigations. Hydrol. Process. 20, 969–985. https://doi.org/10.1002/hyp.6115

Covington, M.D., Banwell, A.F., Gulley, J., Saar, M.O., Willis, I., Wicks, C.M., 2012. Quantifying the effects of glacier conduit geometry and recharge on proglacial hydrograph form. J. Hydrol. 414–415, 59–71. https://doi.org/10.1016/j.jhydrol.2011.10.027

Deline, P., 2009. Interactions between rock avalanches and glaciers in the Mont Blanc massif during the late Holocene. Quat. Sci. Rev. 28, 1070–1083. https://doi.org/10.1016/j.quascirev.2008.09.025

Deline, P., 2005. Change in surface debris cover on Mont Blanc massif glaciers after the 'Little Ice Age' termination. The Holocene 15, 302–309.

Deline, P., 2002. Etude géomorphologique des interactions écroulements rocheux/glaciers dans la haute montagne alpine (verant sud-est du Massif du Mant Blanc).

Deline, P., Gardent, M., Kirkbride, M.P., Le Roy, M., Martin, B., 2012. Geomorphology and dynamics of supraglacial debris covers in the Western Alps, in: Geophysical Research Abstracts, EGU General Assembly. p. 10866.

Dow, C.F., Kavanaugh, J.L., Sanders, J.W., Cuffey, K.M., 2014. A test of common assumptions used to infer subglacial water flow through overdeepenings. J. Glaciol. 60, 725–734. https://doi.org/10.3189/2014JoG14J027

Elvehøy, H., Jackson, M., 2018. Engabreen, in: Kjøllmoen, B. (Ed.), Glaciological Investigations in Norway 2017. Norges vassdrags- og energidirektorat, Oslo, pp. 58–62.

Escher-Vetter, H., Reinwarth, O., 1994. Two decades of runoff measurements (1974 to 1993) at the pegelstation Vernagtbach/Oetztal Alps. Zeitschrift für Gletscherkd. und Glazialgeol. 30, 53–98.

Fairchild, I.J., Bradby, L., Sharp, M., Tison, J.-L., 1994. Hydrochemistry of carbonate terrains in alpine glacial settings. Earth Surf. Process. Landforms 19, 33–54.

Flowers, G.E., 2008. Subglacial modulation of the hydrograph from glacierized basins. Hydrol. Process. 22, 3903–3918. https://doi.org/10.1002/hyp

Flowers, G.E., Clarke, G.K.C., 2002. A multicomponent coupled model of glacier hydrology 1. Theory and synthetic examples. J. Geophys. Res. 107, 2287. https://doi.org/10.1029/2001JB001122

Foster, L.A., Brock, B.W., Cutler, M.E.J., Diotri, F., 2012. A physically based method for estimating supraglacial debris thickness from thermal band remote-sensing data. J. Glaciol. 58, 677–691. https://doi.org/10.3189/2012JoG11J194

715 Fountain, A.G., 1992. Subglacial water flow inferred from stream measurements at South
716 Cascade Glacier, Washington, USA. J. Glaciol. 38, 51–64.

717 Fyffe, C.L., 2012. The hydrology of debris-covered glaciers. University of Dundee.

718 Fyffe, C.L., Brock, B.W., Kirkbride, M.P., Mair, D.W.F., Arnold, N.S., Smiraglia, C.,
719 Diolaiuti, G., Diotri, F., 2019. Do debris-covered glaciers demonstrate distinctive
720 hydrological behaviour compared to clean glaciers? J. Hydrol. 570, 584–597.
721 https://doi.org/10.1016/j.jhydrol.2018.12.069

722 Fyffe, C.L., Reid, T.D., Brock, B.W., Kirkbride, M.P., Diolaiuti, G., Smiraglia, C., Diotri, F.,
723 2014. A distributed energy-balance melt model of an alpine debris-covered glacier. J.
724 Glaciol. 60, 587–602. https://doi.org/10.3189/2014JoG13J148

725 Han, H., Liu, S., Wang, J., Wang, Q., Xie, C., 2010. Glacial runoff characteristics of the
726 Koxkar Glacier, Tuomuer-Khan Tengri Mountain Ranges, China. Environ. Earth Sci.
727 61, 665–674. https://doi.org/10.1007/s12665-009-0378-9

728 Hannah, D.M., Gurnell, A.M., Mcgregor, G.R., 1999. A methodology for investigation of the
729 seasonal evolution in proglacial hydrograph form. Hydrol. Process. 13, 2603–2621.

730 Hannah, D.M., Smith, B.P.G., Gurnell, A.M., McGregor, G.R., 2000. An approach to
731 hydrograph classification. Hydrol. Process. 14, 317–338.

732 Hasnain, S.I., Thayyen, R.J., 1999a. Controls on the major-ion chemistry of the Dokriani
733 glacier meltwaters, Ganga basin, Garhwal Himalaya, India. J. Glaciol. 45, 87–92.

734 Hasnain, S.I., Thayyen, R.J., 1999b. Discharge and suspended-sediment concentration of
735 meltwaters, draining from the Dokriani glacier, Garhwal Himalaya, India. J. Hydrol.
736 218, 191–198. https://doi.org/10.1016/S0022-1694(99)00033-5

737 Hasnain, S.I., Thayyen, R.J., 1994. Hydrograph seperation of bulk melt-waters of Dokriani
738 Bamak glacier basin, based on electrical conductivity. Curr. Sci. 67, 189–193.

739 Hawkings, J., Wadham, J., Tranter, M., Telling, J., Bagshaw, E., Beaton, A., Simmons, S.-L.,
740 Chandler, D., Tedstone, A., Nienow, P., 2016. The Greenland Ice Sheet as a hot spot of
741 phosphrus weathering and export in the Arctic. Global Biogeochem. Cycles 30, 191–
742 210. https://doi.org/10.1002/2015GB005237

743 Hodgkins, R., 2001. Seasonal evolution of meltwater generation, storage and discharge at a
744 non-temperate glacier in Svalbard. Hydrol. Process. 15, 441–460.
745 https://doi.org/10.1002/hyp.160

746 Hodgkins, R., Tranter, M., Dowdeswell, J.A., 1998. The hydrochemistry of runoff from a
747 ‘cold-based’ glacier in the High Artic (Scott Turnerbreen, Svalbard). Hydrol. Process.
748 12, 87–103.

749 Hodson, A., Mumford, P., Lister, D., 2004. Suspended sediment and phosphorous in
750 proglacial rivers: Bioavailability and potential impacts upon the P status of ice-marginal
751 receiving waters. Hydrol. Process. 18, 2409–2422. https://doi.org/10.1002/hyp.1471

752 Hodson, A., Porter, P., Lowe, A., Mumford, P., 2002. Chemical denudation and silicate
753 weathering in Himalayan glacier basins: Batura Glacier, Pakistan. J. Hydrol. 262, 193–
754 208. https://doi.org/10.1016/S0022-1694(02)00036-7

755 Hodson, A.J., Gurnell, A.M., Washington, R., Tranter, M., Clark, M.J., Hagen, J.O., 1998.
756 Meteorological and runoff time-series characteristics in a small, high-Arctic glaciated
757 basin, Svalbard. Hydrol. Process. 12, 509–526.

758 Hubbard, B., Glasser, N., 2005. Field Techniques in Glaciology and Glacial Geomorphology.

John Wiley and Sons Ltd, Chichester.

Hubbard, B.P., Sharp, M.. J., Willis, I.C., Nielsen, M.K., Smart, C.C., 1995. Borehole water-level variations and the structure of the subglacial hydrological system of Haut Glacier d'Arolla, Valais, Switzerland. J. Glaciol. 41, 572–583.

Irvine-Fynn, T.D.L., Porter, P.R., Rowan, A. V., Quincey, D.J., Gibson, M.J., Bridge, J.W., Watson, C.S., Hubbard, A., Glasser, N.F., 2017. Supraglacial Ponds Regulate Runoff From Himalayan Debris-Covered Glaciers. Geophys. Res. Lett. 44, 11,894-11,904. https://doi.org/10.1002/2017GL075398

Jobard, S., Dzikowski, M., 2006. Evolution of glacial flow and drainage during the ablation season. J. Hydrol. 330, 663–671. https://doi.org/10.1016/j.jhydrol.2006.04.031

Kirkbride, M.P., Deline, P., 2013. The formation of supraglacial debris covers by primary dispersal from transverse englacial debris bands. Earth Surf. Process. Landforms 38, 1779–1792. https://doi.org/10.1002/esp.3416

Kirkbride, M.P., Dugmore, A.J., 2003. Glaciological response to distal tephra fallout from the 1947 eruption of Hekla, south Iceland. J. Glaciol. 49, 420–428.

Kjøllmoen, B., 2018. Nigardsbreen, in: Kjøllmoen, B. (Ed.), Glaciological Investigations in Norway 2017. Norges vassdrags- og energidirektorat, Oslo, pp. 28–31.

Kumar, K., Miral, M.S., Joshi, S., Pant, N., Joshi, V., Joshi, L.M., 2009. Solute dynamics of meltwater of Gangotri glacier, Garhwal Himalaya, India. Environ. Geol. 58, 1151–1159. https://doi.org/10.1007/s00254-008-1592-6

Lambrecht, A., Mayer, C., Hagg, W., Popovnin, V., Rezepkin, A., Lomidze, N., Svanadze, D., 2011. A comparison of glacier melt on debris-covered glaciers in the northern and southern Caucasus. Cryosph. 5, 525–538. https://doi.org/10.5194/tc-5-525-2011

Li, S., Yao, T., Yang, W., Yu, W., Zhu, M., 2016. Melt season hydrological characteristics of the Parlung No. 4 Glacier, in Gangrigabu Mountains, south-east Tibetan Plateau. Hydrol. Process. 30, 1171–1191. https://doi.org/10.1002/hyp.10696

Liu, W., Ren, J., Qin, X., Liu, J., Liu, Q., Cui, X., Wang, Y., 2010. Hydrological characteristics of the Rongbuk Glacier catchment in Mt. Qomolangma region in the central Himalayas, China. J. Mt. Sci. 7, 146–156. https://doi.org/10.1007/s11629-010-1069-4

Maisch, M., Haeberli, W., Hoelzle, M., Wenzel, J., 1999. Occurrence of rocky and sedimentary glacier beds in the Swiss Alps as estimated from glacier-inventory data. Ann. Glaciol. 1973, 231–235.

Mattson, L.E., Gardner, J.S., Young, G.J., 1993. Ablation on Debris Covered Glaciers: an Example from the Rakhiot Glacier, Punjab, Himalaya, in: Snow and Glacier Hydrology, IAHS Publication. pp. 289–296.

Maurya, A.S., Shah, M., Deshpande, R.D., Bhardwaj, R.M., Prasad, A., Gupta, S.K., 2011. Hydrograph separation and precipitation source identification using stable water isotopes and conductivity: River Ganga at Himalayan foothills. Hydrol. Process. 25, 1521–1530. https://doi.org/10.1002/hyp.7912

Miles, E.S., Steiner, J., Willis, I., Buri, P., Immerzeel, W.W., Chesnokova, A., Pellicciotti, F., 2017. Pond Dynamics and Supraglacial-Englacial Connectivity on Debris-Covered Lirung Glacier, Nepal. Front. Earth Sci. 5. https://doi.org/10.3389/feart.2017.00069

Miles, K.E., Hubbard, B., Quincey, D.J., Miles, E.S., Irvine-fynn, T.D.L., Rowan, A. V, 2019. Surface and subsurface hydrology of debris-covered Khumbu Glacier , Nepal ,

804 revealed by dye tracing. Earth Planet. Sci. Lett. 513, 176–186.
805 https://doi.org/10.1016/j.epsl.2019.02.020

806 Milner, A.M., Khamis, K., Battin, T.J., Brittain, J.E., Barrand, N.E., Füreder, L., Cauvy-
807 Fraunié, S., Gíslason, G.M., Jacobsen, D., Hannah, D.M., Hodson, A.J., Hood, E.,
808 Lencioni, V., Ólafsson, J.S., Robinson, C.T., Tranter, M., Brown, L.E., 2017. Glacier
809 shrinkage driving global changes in downstream systems. Proc. Natl. Acad. Sci. 114,
810 9770–9778. https://doi.org/10.1073/pnas.1619807114

811 Nicholson, L., Benn, D.I., 2006. Calculating ice melt beneath a debris layer using
812 meteorological data. J. Glaciol. 52, 463–470.
813 https://doi.org/10.3189/172756506781828584

814 Østrem, G., 1959. Ice melting under a thin layer of moraine, and the existance of ice cores in
815 moraine ridges. Geogr. Ann. 41, 228–230.

816 Pavan, M., Smiraglia, C., Merlanti, F., 1999. Prospezione geofisca sul ghiacciaio del Miage
817 (Alpi accidentali).

818 Rainwater, F.H., Guy, H.P., 1961. Some Observations on the Hydrochemistry and
819 Sedimentation of the Chamberlin Glacier Area Alaska, Geological Survey Professional
820 Paper 414-C.

821 Raiswell, R., 1984. Chemical models of solute aquisition in glacial meltwaters. J. Glaciol. 30,
822 49–57. https://doi.org/10.1017/S0022143000008480

823 Raiswell, R., Thomas, A.G., 1984. Solute acquisition in glacial melt waters I. Fjallsjökull
824 (south-east Iceland): bulk melt waters with closed-system characteristics. J. Glaciol. 30,
825 35–43.

826 Reid, T.D., Brock, B.W., 2010. An energy-balance model for debris-covered glaciers
827 including heat conduction through the debris layer. J. Glaciol. 56, 903–916.
828 https://doi.org/10.3189/002214310794457218

829 RGI Consortium, 2017. Randolph Glacier Inventory – A Dataset of Global Glacier Outlines:
830 Version 6.0: Technical Report. https://doi.org/https://doi.org/10.7265/N5-RGI-60

831 Ruffles, L.M., 1999. In situ investigations of subglacial hydrology and basal ice at Svartisen
832 Glaciological Observatory, Norway. University of Wales, Aberystwyth.

833 Scherler, D., Bookhagen, B., Strecker, M.R., 2011. Spatially variable response of Himalayan
834 glaciers to climate change affected by debris cover. Nat. Geosci. 4, 156–159.

835 Scherler, D., Wulf, H., Gorelick, N., 2018. Global Assessment of Supraglacial Debris-Cover
836 Extents. Geophys. Res. Lett. 45, 11798–11805. https://doi.org/10.1029/2018GL080158

837 Singh, P., Haritashya, U.K., Kumar, N., 2004. Seasonal changes in meltwater storage and
838 drainage characteristics of the Dokriani Glacier, Garhwal Himalayas (India). Hydrol.
839 Res. 35, 15–29.

840 Singh, P., Haritashya, U.K., Kumar, N., Singh, Y., 2006. Hydrological characteristics of the
841 Gangotri Glacier, central Himalayas, India. J. Hydrol. 327, 55–67.
842 https://doi.org/10.1016/j.jhydrol.2005.11.060

843 Singh, P., Ramasastri, K.S., Singh, U.K., Gergan, J.T., Dobhal, D.P., 1995. Hydrological
844 characteristics of the Dokriani Glacier in the Garhwal Himalayas. Hydrol. Sci. 40, 243–
845 257.

846 Song, G., Wang, N., Chen, L., He, J., Jiang, X., Wu, X., 2008. Analysis of the Recent
847 Features of the Meltwater Runoff from the Qiyi Glacier, Qilian Mountains (in Chinese).

J. Glaciol. Geocryol. 30, 321–328.

Srivastava, D., Kumar, A., Verma, A., Swaroop, S., 2014. Analysis of Climate and Melt-runoff in Dunagiri Glacier of Garhwal Himalaya (India). Water Resour. Manag. 28, 3035–3055. https://doi.org/10.1007/s11269-014-0653-8

Steinpórsson, S., Óskarsson, N., 1983. Chemical monitoring of Jökulhlaup water in Skeidará and the geothermal system in Grímsvötn, Iceland. Jökull 33, 73–86.

Stokes, C.R., Popovnin, V., Aleynikov, A., Gurney, S.D., Shahgedanova, M., 2007. Recent glacier retreat in the Caucasus Mountains, Russia, and associated increase in supraglacial debris cover and supra-/proglacial lake development. Ann. Glaciol. 46, 195–203.

Swift, D.A., Nienow, P.W., Hoey, T.B., Mair, D.W.F., 2005. Seasonal evolution of runoff from Haut Glacier d'Arolla, Switzerland and implications for glacial geomorphic processes. J. Hydrol. 309, 133–148. https://doi.org/10.1016/j.jhydrol.2004.11.016

Tranter, M., Brown, G., Raiswell, R., Sharp, M., Gurnell, A., 1993a. A conceptual model of solute acquisition by Alpine glacial meltwaters. J. Glaciol. 39, 573–581.

Tranter, M., Brown, G.H., Hodson, A.J., Gurnell, A.M., 1996. Hydrochemistry as an indicator of subglacial drainage system structure: a comparison of alpine and sub-polar environemtents. Hydrol. Process. 10, 541–556.

Tranter, M., Brown, G.H., Sharp, M.J., 1993b. The use of sulphate as a tracer for the delayed flow component of alpine glacier runoff, in: Tracers in Hydrology, IAHS Publication No. 215. pp. 89–177.

Tranter, M., Raiswell, R., 1991. The composition of the englacial and subglacial component in bulk meltwaters draining Gornergletscher, Switzerland. J. Glaciol. 37, 59–66.

VAW/ETHZ and EKK/SCNAT, 2018. Glaciological reports (1881-2017) "The Swiss Glaciers".

Wang, L., Li, Z., Wang, F., Edwards, R., 2014. Glacier shrinkage in the Ebinur lake basin, Tien Shan, China, during the past 40 years. J. Glaciol. 60, 245–254. https://doi.org/10.3189/2014JoG13J023

Willis, I.C., Arnold, N.S., Brock, B.W., 2002. Effect of snowpack removal on energy balance, melt and runoff in a small supraglacial catchment. Hydrol. Process. 16, 2721–2749. https://doi.org/10.1002/hyp.1067

Xie, C., Ding, Y., Liu, S., Chen, C., 2006. Response of meltwater runoff to air-temperature fluctuations on Keqikaer glacier, south slope of Tuomuer mountain, western China. Ann. Glaciol. 43, 275–279.

Xu, J., Grumbine, R.E., Shrestha, A., Eriksson, M., Yang, X., Wang, Y., Wilkes, A., 2009. The melting Himalayas: cascading effects of climate change on water, biodiversity, and livelihoods. Conserv. Biol. 23, 520–30. https://doi.org/10.1111/j.1523-1739.2009.01237.x

Supplementary Information

A Stage-discharge rating

In total 29 dilution gaugings were conducted using Rhodamine WT within the 2010 and 2011 field seasons (Table A). However some gaugings were excluded from the rating due to either less accurate measurement of the injected dye quantities (June 2010) or less clear dye breakthrough curves, so that 19 gaugings covering flows from P(99) to P(19) were used to construct the rating (exceedance values based on the short term flow duration curve derived from both years of data). The stages for all gaugings were adjusted to the position of the June 2010 well, necessary given that a sufficient range of flows was not always captured within each field visit to produce separate ratings. Although the large boulders acting as a control on the water level at the stilling well could have shifted during high flows, the gaugings from the different time periods did correspond when similar flows were measured. A two-part rating curve (Figure A) was constructed using the standard form:

$$Q = x(h + z)^{y}, \quad (1)$$

Where Q is discharge ($m^3 s^{-1}$), h is stage (ma SD) and x, y and z are coefficients as detailed in Table B which differ for each part of the curve. A two-part rating was chosen as a single equation underestimated the discharge at low stages. There is some disparity between the included gaugings at high flows but here the excluded gaugings match the rating well, with the highest excluded flow gauging equal to P(6). The rating has a standard error of the estimate of 0.76 $m^3 s^{-1}$, which gives a percentage error of 14.6% using the average daily discharge in 2010 of 5.37 m^3

910 Table A Proglacial stream dilution gaugings.

Date	Start Time	Stage (ma SD)	Discharge ($m^3 s^{-1}$)	Exceedance (%ile)	Used in rating?
07/06/2010	16:35	0.405	5.147	50	n
13/06/2010	11:18	0.426	9.643	14	n
15/06/2010	16:39	0.377	3.983	63	n
20/06/2010	11:03	0.328	1.247	99.9	n
21/06/2010	13:59	0.271	1.830	97	n
02/08/2010	11:21	0.525	11.807	7	n
02/08/2010	13:25	0.541	12.147	6	n
02/08/2010	16:20	0.545	8.776	18	n
06/08/2010	09:55	0.360	2.068	90	y
04/09/2010	17:05	0.427	4.815	54	y
08/09/2010	12:43	0.397	3.767	65	y
08/09/2010	14:55	0.397	4.050	63	y
08/09/2010	16:49	0.399	4.220	61	y
09/09/2010	09:44	0.276	3.174	71	n
10/09/2010	09:51	0.262	2.678	77	n
04/06/2011	12:43	0.362	2.300	82	y
07/06/2011	12:07	0.308	1.679	99	y
12/06/2011	11:46	0.319	2.268	83	y
12/06/2011	18:19	0.356	2.224	85	y
14/06/2011	10:42	0.344	2.202	85	y
14/06/2011	18:42	0.384	2.498	79	y
31/07/2011	09:00	0.424	6.606	35	y
31/07/2011	17:23	0.444	8.538	19	y
03/08/2011	10:40	0.485	8.252	21	n
04/08/2011	08:52	0.474	8.993	17	n
04/08/2011	15:33	0.516	10.325	11	n
12/09/2011	14:11	0.471	6.730	34	y
15/09/2011	09:36	0.397	3.892	64	y
15/09/2011	17:29	0.421	4.508	57	y

911 Table B Rating coefficients.

Applied to stages	***x***	***y***	***y***
<0.366 ma SD	7.73	1.3	0.029
≥0.366 ma SD	80.81	1.3	-0.301

912

913

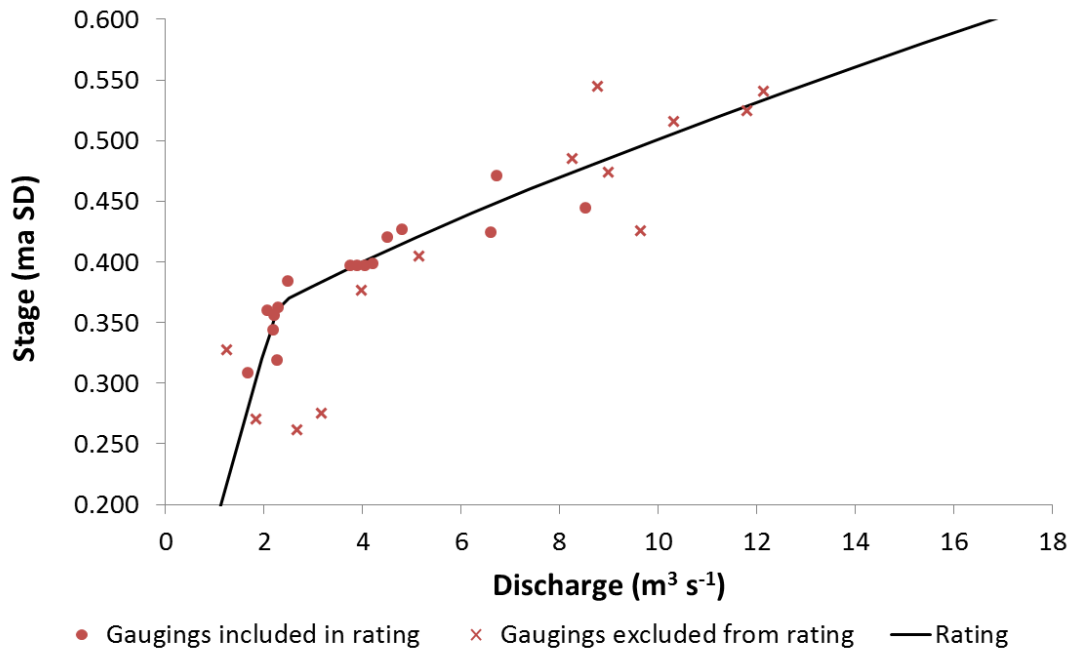

914

915 Figure A Rating curve for proglacial stream. Details of the gaugings are given in Table A.

916

917 **B Quantifying the 'debris delay'**

918 The time of peak melt from each surface cover type (as determined by Fyffe et al. (2014)) can
919 be used to determine the average delay due to the conduction of heat through the debris. The
920 time of peak melt was 13:00 for clean snow and ice, 14:00 for dirty ice and 15:00 for debris-
921 covered ice – therefore on average the conduction of heat through the debris causes a 1-2
922 hour delay. The delay due to the less efficient englacial/subglacial system in the debris-
923 covered area can be quantified using dye tracing results. The average travel time to the snout
924 (around 3.5 hours) is the same from the debris-covered and clean ice areas (based on the
925 mean dye velocities from the debris-covered (0.26 m s^{-1}) and clean/dirty ice (0.56 m s^{-1}) areas
926 and the distance to the centroid of these cover types (3304 m and 7149 m, respectively)
927 (Fyffe et al., 2019). If sub-debris meltwater was transferred at the speed of the more efficient
928 system then the travel time would be only 1.6 hours. The less efficient englacial/subglacial
929 system therefore adds a 1.9 hour delay.

930

931

932 Table 1 Summary of relevant papers addressing the water chemistry and proglacial runoff
933 characteristics of debris-covered glaciers. Key characteristics of the glaciers mentioned are
934 given in Table 10. *The Parlung No. 4 Glacier is not debris-covered but the paper has been

included since it mentions findings related to debris-covered glaciers in the Tibetan region. The current paper is added for completeness.

Study	Location (only debris-covered glaciers)	Focus	Key Results
This study.	Miage Glacier, Italian Alps	Proglacial runoff, solute and SSC	SSC and bicarbonate concentrations are enhanced by the supraglacial debris. The inefficient subglacial system (itself a result of the debris cover) increases the bicarbonate ad sulphate concentrations compared to clean glaciers. The baseflow component of discharge and the lag time between peak air temperature and discharge are increased due to the delaying effects of the debris. Clearly diurnal hydrographs are also confined to periods of warmer weather.
Han et al. (2010)	Koxkar Glacier, China	Proglacial runoff	Seasonal runoff variability is greater than annual, with maximum discharge in August. Maximum runoff is 1800-0200 with minimum 0700-1000. Lag time between peak melt and discharge varies between 4 and 10 hrs.
Hasnain and Thayyen (1994)	Dokriani Glacier, Garhwal Himalaya	Proglacial runoff and solute	Used conductivity measurements to separate the hydrograph into englacial and subglacial components. Conductivity varied diurnally and out of phase with discharge.
Hasnain and Thayyen (1999a)	Dokriani Glacier, Garhwal Himalaya	Proglacial runoff, solute and SSC	The chemical-denudation rate was particularly high, indicating intense chemical weathering. Chemical weathering likely dominated by coupled reactions of sulphide oxidation and carbonate dissolution. Monsoonal rainfall thought to enhance weathering of supraglacial debris and result in high proglacial concentrations of sulphate.
Hasnain and Thayyen (1999b)	Dokriani Glacier, Garhwal Himalaya	Proglacial runoff and SSC	The majority of runoff, suspended sediment transport and rainfall occurred during the monsoon months of July and August. The timing of discharge and SSC peak became progressively earlier in the day over the ablation season.
Hodson et al. (2002)	Batura Glacier, Pakistan	Solute dynamics	The majority of solute is derived from carbonate weathering. Chemical denudation is responsible for 75% of the solute yield with rates high and similar to the upper limits for temperate glaciers. The silicate-derived cation denudation rate is also high, likely due to ablation and intense monsoon precipitation causing high flushing rates.
Irvine-Fynn et al. (2017)	Khumbu Glacier, Nepal	Supraglacial lake runoff	Supraglacial ponds act as storage reservoirs and modulate proglacial discharge, with ponds storing >23% of mean daily discharge. As supraglacial pond and debris cover extent increases the authors expect the runoff signal to become further attenuated.
Kumar et al. (2009)	Gangotri Glacier, Garwhal Himalaya	Solute dynamics	The dominant cations were found to be magnesium and calcium with bicarbonate and sulphate the dominant anions. Carbonate weathering mainly controls the meltwater chemistry. Inverse relationships are found between discharge and some cations, but the relationships are weak, possibly due to high flow events corresponding with rising cation concentrations.
Li et al. (2016)	Parlung No. 4 Glacier*	Proglacial runoff	Air temperature, vapour pressure and incoming shortwave radiation were significantly positively correlated with discharge. Daily discharge could be simulated from a multiple regression model. Most discharge occurred in July and August with the daily discharge cycle altering over the season. Differences in the inter-annual proglacial discharge characteristics were found between glaciers in the Tibetan Plateau. These differences are explained by the existence of debris cover on some glaciers.

Liu et al. (2010)	Rongbuk Glacier, Central Himalaya	Proglacial runoff	The high nighttime discharges suggested significant storage, explained by the large glacier area and existence of glacier lakes. The time lag between maximum daily air temperature and discharge ranged from 8 to 14 hours, with this time reducing over the season. Air temperature correlated well with discharge. Most runoff occurred between April and October.
Singh et al. (1995)	Dokriani Glacier, Garhwal Himalaya	Proglacial runoff, SSC and water temperature	Analysis of the proglacial runoff included determination of mean amplitude, recession analysis and peak timing. Discharge and SSC did not have a significant relationship. Runoff and air temperature were significantly correlated suggesting that solely air temperature could be used for future melt modelling.
Singh et al. (2004)	Dokriai Glacier, Garwhal Himalaya	Proglacial runoff	Nighttime discharges are high and comparable to daytime discharges throughout the season, explained by storage which is more significant earlier in the season. Diurnal variations become clearer over the season, with the amplitude greatest in August. Lag times between peak air temperature and discharge ranged between 3-6 hours, shortening over the ablation season.
Singh et al. (2006)	Gangotri Glacier, Garwhal Himalaya	Proglacial runoff	Proglacial runoff is highest in July, but with maximum diurnal variability in May and September. Daytime and nighttime runoff magnitudes are similar, demonstrating the strong storage characteristics of the glacier. The time lag from peak air temperature to peak discharge varied from 4 to 7.30 hrs. The relationship between air temperature and discharge was stronger on a monthly rather than daily timescale.

Table 2 Guide to fieldwork dates and data collected. 'Water Chemistry', 'Discharge' and 'Conductivity' measurements were of the proglacial stream and were not necessarily continuous throughout these periods (see individual sections for details).

Year	Months	Start day	End day	Measurements
2010	June	05/06/2010	24/06/2010	Water Chemistry
	July/Aug	28/07/2010	06/08/2010	Water Chemistry
	Sep	04/09/2010	10/09/2010	Water Chemistry
	June-Sep	05/06/2010	12/09/2010	Discharge, Conductivity
	June-Sep	05/06/2010	13/09/2010	Meteorology
2011	June	04/06/2011	15/06/2011	Water Chemistry
	July/Aug	26/07/2011	04/08/2011	Water Chemistry
	Sep	12/09/2011	15/09/2011	Water Chemistry
	June-Sep	04/06/2011	16/09/2011	Discharge, Conductivity
	June-Oct	04/06/2011	11/10/2011	Meteorology

945 Table 3 Details of proglacial stream and water chemistry instruments.

Quantity	Location	Time period	Manufacturer	Type	Accuracy
Stage	Proglacial	2010 and June 2011	GE Sensing	Druck PTX1830 (vented)	±0.1% full scale (or ±0.06% full scale)
	Proglacial	Aug and Sep 2011	Onset	HOBO U20 - 001-04 (non-vented)	±0.075% full scale, ±0.3 cm
Fluorescence	Proglacial	2010 and June 2011	Seapoint	Rhodamine fluorometer	Not stated but minimum detection 0.02 ppb
	Proglacial	July, Aug, Sep 2011	Turner	Cyclops-7 Rhodamine	Not stated but minimum detection 0.01 ppb
Conductivity and temperature	Supraglacial	Both years.	Hanna	HI9033 with HI 76302W probe	± 1% full scale (excluding probe)
	Proglacial	Both years.	Campbell	CS547A	±5% of reading 0.44 to 7.0 mS cm^{-1}, ±10% of reading 0.005 to 0.44 mS cm^{-1} ±0.4°C
pH	All	Both years.	Hanna	HI 98140/HI 98128	±0.01 pH
Turbidity	All	Both years	Hanna	HI 93703	±0.5 FTU or 5% whichever is greater

946

947

948

949 Table 4 Water quality data. Values are means where more than one sample was taken although mean proglacial values are of twice daily values
950 and do not include values from hourly sampling on specific days. Where the number of measurements averaged does not equal the number of
951 samples stated (due to instrument failure/unsatisfactory errors in laboratory analysis) the number of measurements is given in brackets. 'S' streams
952 were also dye injection streams, whereas 'WS' streams were used only for water chemistry measurements. 'SP' refers to small ponds whereas the
953 lakes were much larger (diameter of tens of metres). Q is the stream discharge (either of the supraglacial or proglacial stream depending on the
954 sample location), and u_s is the supraglacial stream velocity.

955

Name	No. of samples	Cond. (µ S cm^{-1})	SSC (mg l^{-1})	pH	Temp. (°C)	HCO^{-}_{3} (µeq l^{-1})	SO^{2-}_{4} (µeq l^{-1})	C-ratio	$p(CO_2)$	Q (m^3 s^{-1})	u_s (m s^{-1})
Proglacial stream samples (averaged over time periods)											
2010	54	66.2 (46)	312	8.2 (50)	0.4 (50)	783 (47)	200 (46)	0.80 (40)	-3.5 (43)	4.19	-
June 2010	33	70.7	381	8.5 (32)	0.4 (32)	856 (28)	204 (26)	0.82 (22)	-3.8 (27)	3.06	-
July/Aug 2010	12	62.4 (6)	242 (12)	7.5 (9)	0.4 (9)	714 (10)	199	0.80 (10)	-3.0 (7)	7.84	-
Sep 2010	9	48.4 (7)	153	7.7	0.3	630	189 (8)	0.76 (8)	-3.2	3.51	-
2011	22	55.5 (13)	146 (21)	8.2 (13)	-	603 (21)	215 (21)	0.74 (21)	-3.9 (12)	4.64	-
June 2011	9	69.0 (4)	106	8.1 (4)	-	608	224	0.73	-3.5 (4)	2.68	-
July/Aug 2011	9	47.2 (5)	172 (8)	7.6 (5)	-	608 (8)	199 (8)	0.76 (8)	-3.4 (4)	6.22	-
Sep 2011	4	52.4	186	9.1	-	580	228	0.73	-4.6	5.49	-
Lake and pond samples (averaged for each location)											
C4 Lake	1	-	17	-	-	314	47	0.87	-	-	-
C8 Lake	2	-	8	-	-	292	30	0.92	-	-	-
SP5 (pond)	1	56.8	15	9.79	2.7	658	87	0.88	-5.27	-	-
Snow samples (average for all samples)											
Snow	3	-	26 (2)	6.70 (1)	-0.3 (1)	145	76 (2)	0.66 (2)	-2.78 (1)	-	-
Supraglacial stream samples (averaged for each location)											
WS1	1	7.6	60	8.39	0.5	254	-	-	-4.28	-	-
WS2	1	14.3	610	8.51	0.4	329	30	0.92	-4.29	-	-
WS3	1	10.2	32	8.48	0.2	299	23	0.93	-4.30	-	-
WS4	1	-	125.6	-	-	299	14	0.95	-	-	-
WS5	2	-	0	-	-	254	57	0.83	-	-	-
S1	1	16.1	266	7.66	0.1	464	2	1.00	-3.29	-	-
S5	4	10.2	54	7.53 (3)	0.6 (2)	258	12	0.96	-3.42 (3)	0.03 (3)	0.17 (3)
S7	4	28.0 (3)	55	8.20	-	408	6	0.98	-3.90 (3)	0.02 (3)	0.26 (3)
S8	1	-	277	-	-	269	21	0.93	-	-	-
S12	4	4.0 (3)	18	7.75 (1)	-	187	10	0.95	-3.73 (1)	0.18	0.46

S14	1	-	1	-	-	135	0	1.00	-	0.53 (5)	1.14 (5)
S15	5	18.4 (3)	32	8.86 (1)		278	6	0.98	-4.71 (1)	0.02 (2)	0.32 (4)

956

957
958
959 Table 5 Parameters calculated for each diurnally classified daily hydrograph. Units of all
960 parameters are $m^3 s^{-1}$, except Q_{dsdamp} which is dimensionless.

Symbol	Parameter
$\mathbf{Q_{damp}}$	Diurnal discharge amplitude (maximum minus minimum runoff)
$\mathbf{Q_{dmax}}$	Diurnal discharge maximum (runoff peak)
$\mathbf{Q_{dmin}}$	Diurnal discharge minimum (either before or after the peak)
$\mathbf{Q_{dmean}}$	Diurnal discharge mean
$\mathbf{Q_{dsdamp}}$	Diurnal discharge standardised amplitude ((maximum flow-minimum flow)/minimum flow)
$\mathbf{Q_{dstd}}$	Diurnal discharge standard deviation

961

962

963
964 Table 6 Comparison of sulphate and bicarbonate ion concentrations between different glaciers.
965 All values are in μeq l^{-1}, with the mean in brackets and the range giving the maximum and
966 minimum values recorded. Grey shading indicates debris-covered glaciers with background

967 data of the comparison glaciers in Table 10. * represents studies cited in Brown (2002). ** note
968 that these values include hourly samples, unlike Table 4.

Glacier	Source	Non-snowpack SO_4^{2-}	HCO_3^-
Miage Glacier, Italy in 2010 (all proglacial samples)	This study.	(202) 97-473**	(777) 344-1186**
Miage Glacier, Italy in 2011 (all proglacial samples)	This study.	(215) 128-323	(603) 494-688
Batura Glacier, Pakistan	Hodson et al. (2002)	160	730
Dokriani Glacier, India (pre monsoon)	Hasnain and Thayyen (1999a)	160-418	159-397
Dokriani Glacier, India (monsoon)	Hasnain and Thayyen (1999a)	85-1140	128-1053
Dokriani Glacier, India (post monsoon)	Hasnain and Thayyen (1999a)	137-431	168-384
Gangotri Glacier, India	Kumar et al. (2009)	(673) 333-1186	(1138) 17-4130
Austre Brøggerbreen, Svalbard	Tranter et al. (1996)	10-140	145-520
Bench Glacier, Alaska	Anderson et al. (2000)*	262	427
Chamberlain, USA	Rainwater and Guy (1961)*	29-310	150-200
Engabreen, Norway	Ruffles (1999)*	0-142	51-675
Fjallsjökull, Iceland	Raiswell and Thomas (1984)*	26-66	190-300
Grimsvötn, Iceland	Steinpórsson and Óskarsson (1983)*	132	573
Haut Glacier d'Arolla, Switzerland	Brown et al. (1996)	30-240	180-460
Nigardsbreen, Norway	Brown (2002)	7-40	1.4-8.5
Scott Turnerbreen, Svalbard	Hodgkins et al. (1998)	(130) 96-200	(170) 110-260
Scott Turnerbreen, Svalbard (icing)	Hodgkins et al. (1998)	(830) 0-3200	(1800) 350-4600
Tsanfleuron, Switzerland	Fairchild et al. (1994)*	118	627

969

970

971

972 Table 7 Hydrograph shape classification statistics for selected glaciers, with 'N' the number
973 of hydrographs and '%' the percentage of total. Thirteen hydrographs were not classified in
974 2010 (15%) and 4 in 2011 (7%). Only Miage Glacier is debris-covered. See Table 10 for
975 background data on the comparison glaciers.

Hydrograph shape classifications	**Miage Glacier**				**Haut Glacier d'Arolla (1989: Hannah et al. (2000), 1998 and 1999: Swift et al. (2005))**						**Taillon Glacier (Hannah et al., 1999)**	
Year	2010		2011		1989		1998		1999		1995+1996	
	N	%	N	%	N	%	N	%	N	%	N	%
Rising (*Building/Late Peaked)	26	36	20	38	36*	39*	21	13	30	19	37*	33*
Falling/Recession	15	21	7	13	7	8	27	17	28	18	12	11
Peaked Falling/Peaked Recession					2	2	11	7	5	3		
Peaked/Diurnal Attenuated	32	44	25	48	47 1	51 1	97	62	91	59	56 8	50 7

976

977 Table 8 Hydrograph statistics for Miage Glacier runoff for individual months and phases.
978 Values given are for diurnally classified hydrographs only except where values are given in
979 brackets which are for all hydrographs.

Phase/Period	**Q_{damp} (m^3 s^{-1})**		**Q_{dsdamp} (m^3 s^{-1})**		**Q_{dmax}/Q_{dmin}**	
Year	2010	2011	2010	2011	2010	2011
June	1.66	0.40	0.56	0.20	1.56	1.20
July	5.00	-	1.62	-	2.62	-
Aug	3.03	4.91	0.62	0.83	1.62	1.83
Sep	1.06	3.19	0.32	0.99	1.32	1.99
Phase 1	1.66	0.40	0.56	0.20	1.56	1.20
Phase 2	5.00	4.99	1.62	0.77	2.62	1.77
Phase 3 (2010)	2.67 (3.86)		0.60		1.60	
Phase 3a (2011)		6.03 (4.09)		1.12		2.12
Phase 3b (2011)		3.05 (3.00)		0.89		1.89
Mean	3.41 (3.60)	3.62 (3.39)	1.01	0.70	2.01	1.70

980

981

982 Table 9 Q_{dmax}/Q_{dmin} values for selected glaciers. Debris-covered glaciers are shaded grey with
983 background data of the comparison glaciers in Table 10.

Glacier	Year	Reference	Q_{dmax}/Q_{dmin}						
			May	June	July	Aug	Sep	Oct	Mean
Miage	2010	This study.	-	1.56	2.62	1.62	1.32	-	2.01
Miage	2011	This study.	-	1.2	-	1.83	1.99	-	1.7
Dokriani	1996-1998	Singh et al. (2004, cited in Li et al., 2016)	-	1.3	1.5	2.3	1.7	-	1.7
Dunagiri	1987-1989	(Srivastava et al., 2014)	-	-	1.1	1.1	1.1	-	1.1
Gangotri	2000-2003	(Singh et al., 2006)	1.1	1.2	1.4	1.3	1.2	1.1	1.2
Parlung No. 4	2008/2010-2012	(Li et al., 2016)	2.3	2.2	2.2	2.2	2.4	6.3	2.9
Qiyi	2006	Song et al. (2008, cited in Li et al., 2016)	-	-	-	9	9	-	9

984

Table 10 Background information on glaciers used for comparison in Tables 1, 6, 7, 9, 11 and 12. Glaciers with a substantial debris cover (which covers the full width of the ablation zone) are shaded grey. *The original sources used for comparison were either not available or did not provide the necessary information so alternative sources have been used. The glacier areas and elevations may therefore have changed since the hydrological study referred to in other tables.

Glacier	Country or region	Debris-covered?	Basin area (km^2)	Glacier area (km^2)	Elevation range (m a.s.l.)	Source
Austre Brøggerbreen	Svalbard	n		11	50-720	Tranter et al. (1996)
Batura Glacier	Pakistan	y		365	>7000-~3000	Hodson et al. (2002)
Baounet Glacier	France	n	6	2.5	2800-3300	Jobard and Dzikowski (2006)
Bench Glacier	Alaska	n		8.09	932-1791	RGI Consortium (2017)*
Chamberlain	Alaska	n	3.78	2.41		Rainwater and Guy (1961)
Dokriani Glacier	India	y (75% of ablation area)	9.58	5.76	~4000-6632	Hasnain and Thayyen (1999a)
Dunagiri Glacier	India	y	17.9	2.56	4200-5100	Srivastava et al. (2014)
Engabreen	Norway	n		36	111-1544	Elvehøy and Jackson (2018)*
Fjallsjökull	Iceland	n		63.5	24-2030	RGI Consortium (2017)*
Gangotri Glacier	India	y	556	286	3800-7000	Singh et al. (2006)
Grimsvötn (River Skeiðará)	Iceland	n		1561.2	111-1957	RGI Consortium (2017)* (details for Skeiðarárjökull)
Haut Glacier d'Arolla	Switzerland	n	12	6.3	2560-3838	Brown et al. (1996); Tranter et al. (1996)
Keqikaer Glacier	China	y		83.6	3020-6435	Xie et al. (2006)
Khumbu Glacier	Nepal	y (47% of glacier)		41	4900-8848	Irvine-Fynn et al. (2017)
Koxkar Glacier	China	y (83% of ablation area)		83.56	3060-6342	Han et al. (2010)
Miage Glacier	Italy	y (42% of glacier)	22.7	10.5	1740-4640	This Study
Nigardsbreen	Norway	n		46.6	330-1952	Kjøllmoen (2018)* (area from 2013)
Parlung No. 4 Glacier	China	n	24.3	11.71	4650-5964	Li et al. (2016)
Qiyi	China	n	6.8	2.9		Song et al. (2008, cited in Li et al., 2016)
Rongbuk Glacier	China	y	298	203	5070-8848	Liu et al. (2010)
Scott Turnerbreen	Svalbard	n	12.8	3.3	230-680	Hodgkins et al. (1998)
Taillon Glacier	France	n	0.37	0.22	2526-3022	Hannah et al. (1999)
Tsanfleuron	Switzerland	n		3.81		VAW/ETHZ and EKK/SCNAT (2018)* (area for 1973)

990

991

992 Table 11 Maximum and minimum lag times for selected glaciers derived using analysis of
993 diurnal hydrographs. Debris-covered glaciers are shaded grey with background data of the
994 comparison glaciers in Table 10. *Cited in Li et al. (2016). **Lag time analysis was only
995 conducted for June 2005 so mean, maximum and minimum lag times are from within June.

Glacier	**Year**	**Reference**	**Mean lag time T_{max} to Q_{dmax} (hours)**	**Max. lag time T_{max} to Q_{dmax} (hours)**	**Phase of max. lag time**	**Min. lag time T_{max} to Q_{dmax} (hours)**	**Phase of min. lag time**
Miage Glacier	2010	This study.	6.34	8.43	June/Phase 1	3.63	Aug
Miage Glacier	2011	This study.	7.92	9.67	Sep/Phase 3b	5.5	June/Phase 1
Dokriani Glacier	1996-1998	Singh et al. (2004)*	4.5	6.0	June	3.3	Sep
Gangotri Glacier	2000-2003	Singh et al. (2006)	5.3	6.30-7.30	Oct	4	July
Koxkar Glacier	2005-2008	Han et al. (2010)	7.0	8.80	Oct	5.2	Aug
Rongbuk Glacier	June 2005**	Liu et al. (2010)	10.78	14	9th June	8	10th June
Parlung no. 4 Glacier	2008, 2010-2012	Li et al. (2016)	3.8	14.8	Oct	0.8	July
Qiyi	2006	Song et al. (2008)*	2	-	-	-	-

996

997

998 Table 12 Maximum and minimum lag times for selected glaciers derived using statistical
999 analysis of hydrological and meteorological time series. Debris-covered glaciers are shaded
1000 grey with background data of the comparison glaciers in Table 10. Please see individual studies
1001 for details of the methodology and definition of phases/intervals. *Lag correlations for Baounet
1002 Glacier were conducted using a daily time window rather than phases of several days.

Glacier	Year	Reference	Max. lag time T to Q timeseries (hours)	Phase of max. lag time	Min. lag time T to Q timeseries (hours)	Phase of min. lag time
Miage Glacier	2010	This study.	24	25/07/10-23/08/10/ Aug/Phase 3	7	15/07/10-24/07/10 /July/Phase 2
Keqikaer Glacier	2004	Xie et al. (2006)	25	May	19	June
Austre Brøggerbreen	1991	Hodson et al. (1998)	29	04/07/91-13/07/91/ Phase 2	4	06/08/91-16/08/91/ Phase 5
Austre Brøggerbreen	1992	Hodson et al. (1998)	10	23/06/92-04/07/92/ Phase 1	5	16/07/92-02/08/92/ Phases 4,5,6
Baounet Glacier*	2003	Jobard and Dzikowski (2006)	10	01/06/03 Phase 1	1	end of July-early Aug 2003 Phase 3
Baounet Glacier*	2004	Jobard and Dzikowski (2006)	9	12/06/04 Phase 1	2	mid Aug 2004 Phase 3
Haut Glacier d'Arolla	1998	Swift et al. (2005)	10	02/06/98-07/06/98/ June/Phase 2	0	05/08/98-09/08/98/ Aug/Phase 8
Haut Glacier d'Arolla	1999	Swift et al. (2005)	9	17/06/99-22/06/99/ June/Phase 1	3	20/07/99-23/07/99/ July/Phase 5
Scott Turnerbreen	1992	Hodgkins (2001)	24	11/08/92-17/08/92 Interval 4	1	21/07/92-27/07/92 Interval 1

1003

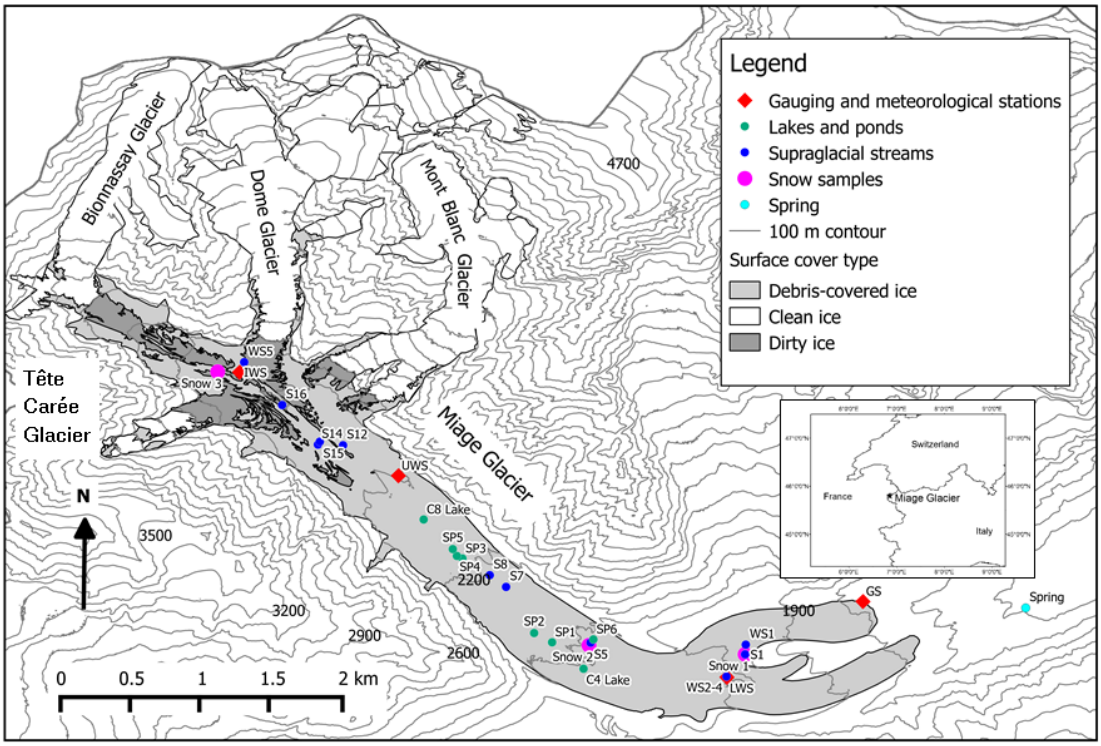

1004

1005 Figure 1 Miage Glacier showing the location of water chemistry samples and gauging and
1006 meteorological stations. Note that 'S' supraglacial streams were also dye traced (see Fyffe et
1007 al. (2019)) whereas 'WS' streams were monitored only for water chemistry purposes. The
1008 prefix 'SP' is for small supraglacial ponds, in distinction to the large lakes (diameter of tens
1009 of metres) at C8 and C4 (GPS locations mentioned in (Fyffe, 2012)).

1010

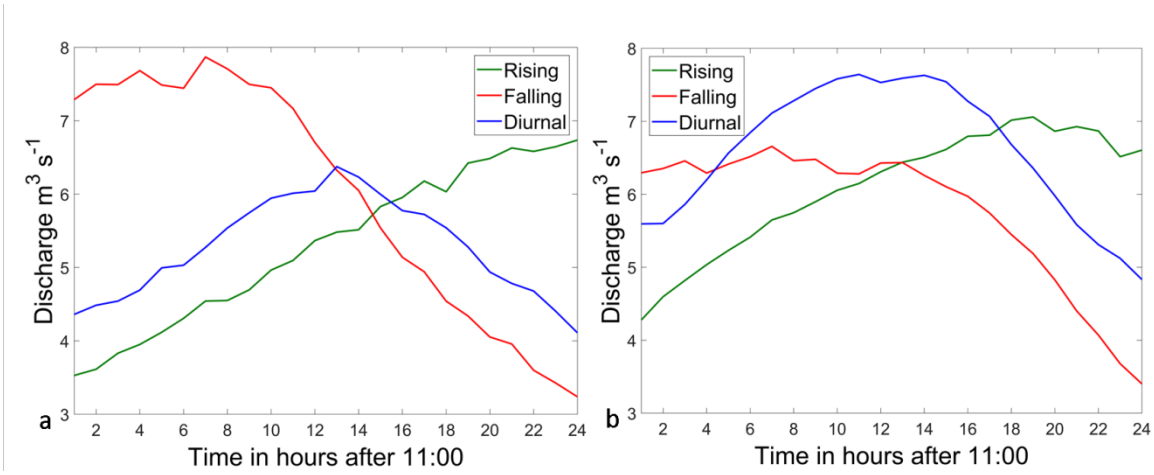

1011

1012 Figure 2 Mean diurnal, rising and falling hydrographs, a) for 2010 and b) for 2011.
1013

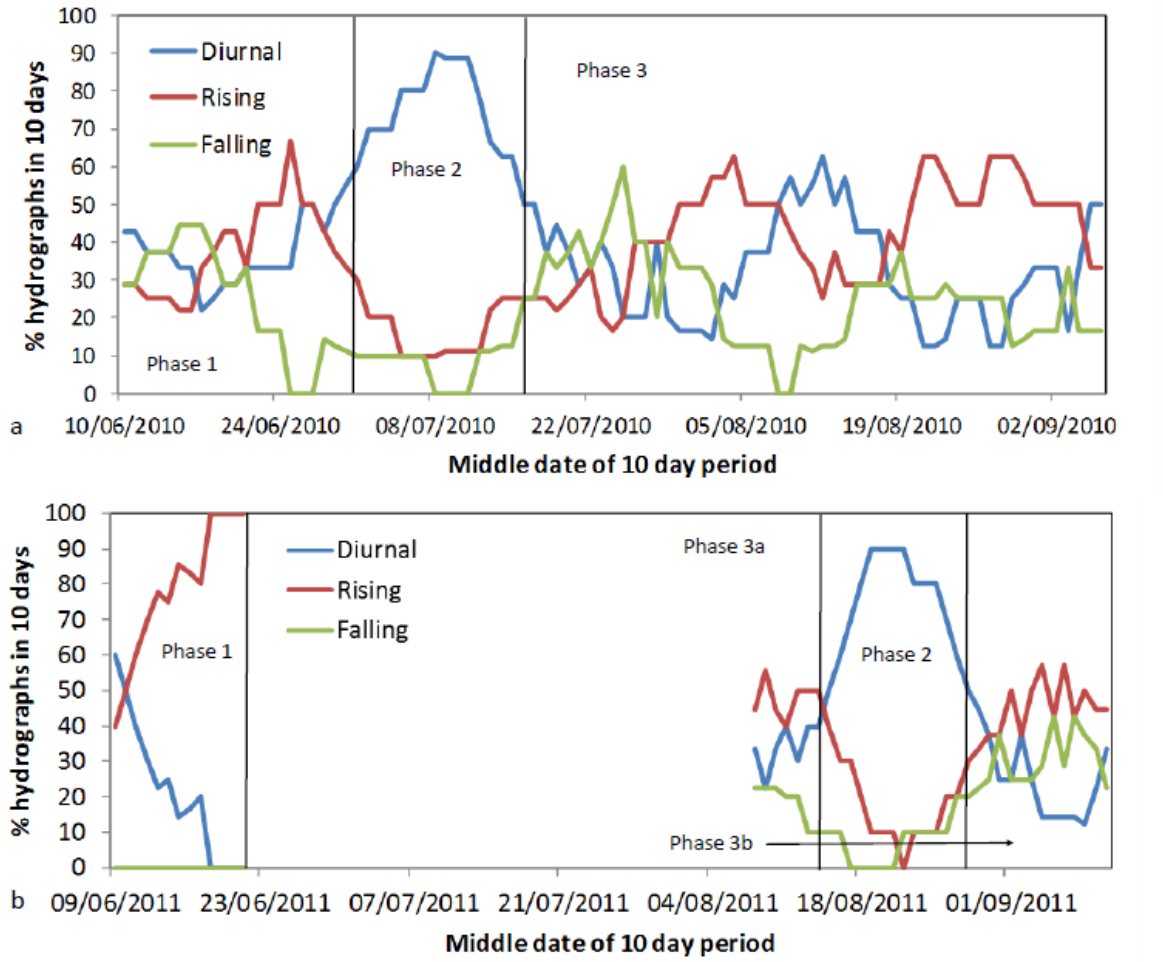

1014
1015 Figure 3 Graph of the % of diurnal, rising or falling hydrographs in running 10 day periods in
1016 a) 2010 and b) 2011.

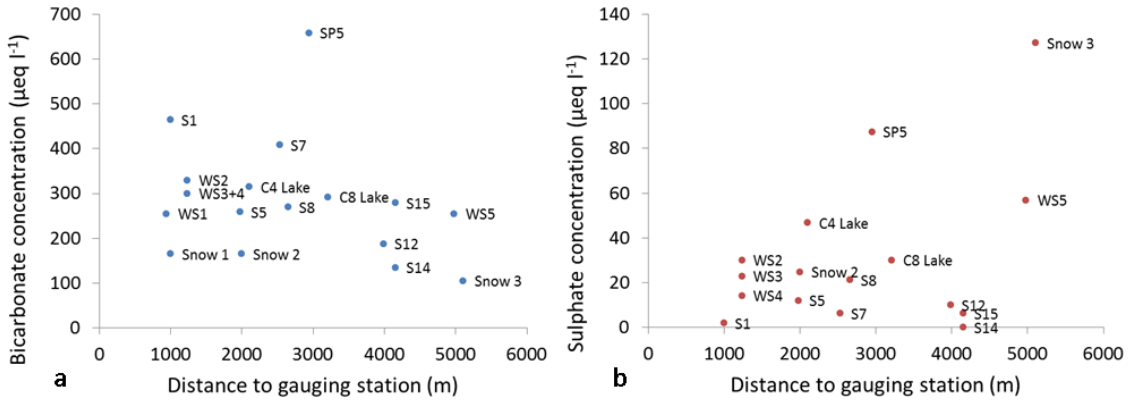

1017

1018 Figure 4 a) bicarbonate and b) sulphate concentration measured from supraglacial locations
1019 plotted against the straight line distance from the gauging station to the sample location.
1020 Some values are averages where more than one sample was taken: see Table 4 for details.

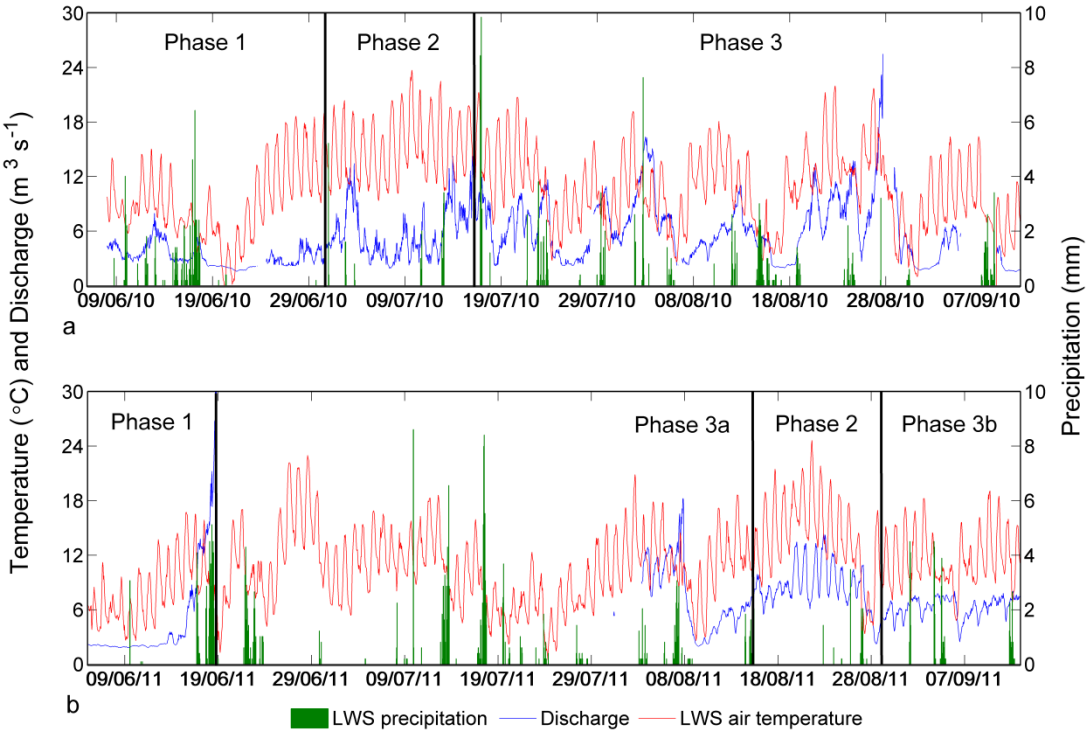

1021

1022 Figure 5 Hourly air temperature and precipitation at LWS and proglacial discharge for a)
1023 2010 and b) 2011. The left y-axis in b has been constrained to 30 m^3 s^{-1} to allow comparison
1024 between years.

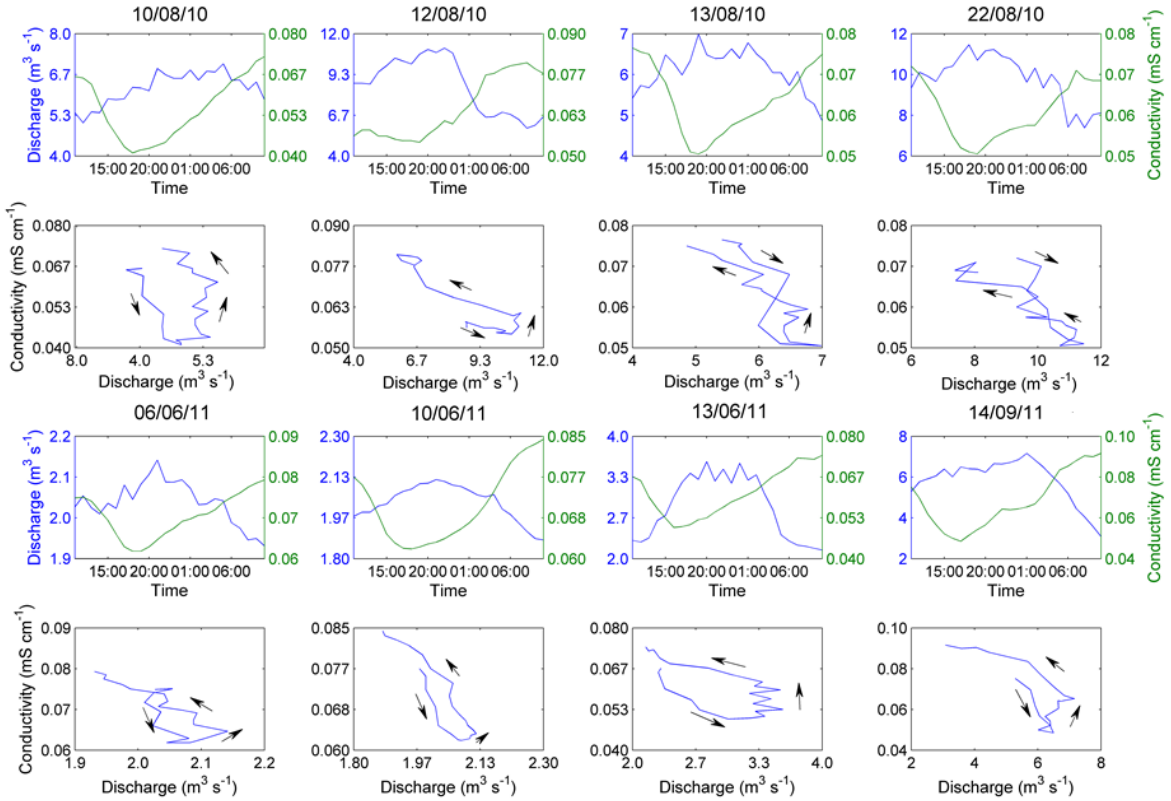

1025

1026 Figure 6 Plots of hourly discharge and conductivity data for days with diurnally classified
1027 discharge and conductivity in 2010 (rows 1 and 2) and 2011 (rows 3 and 4). Note the day
1028 starts at 11:00. The temporal relationship between hourly discharge and conductivity is given
1029 below the time series plots.

1030

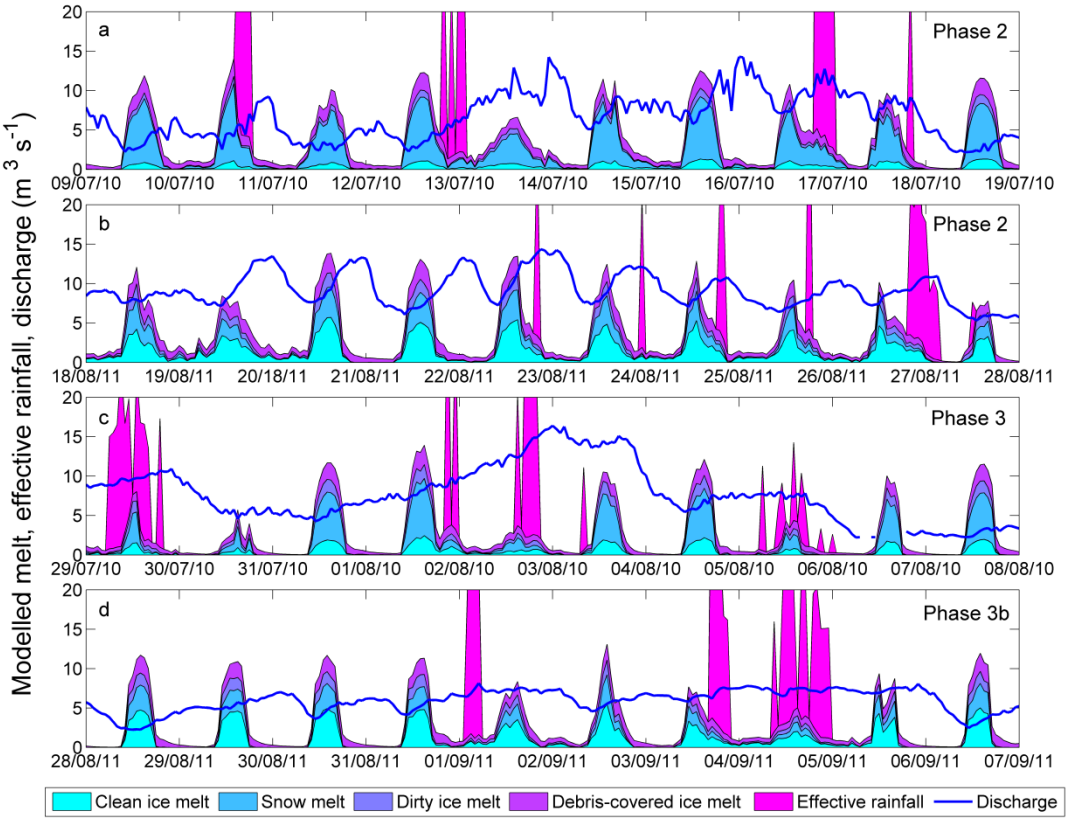

1031

1032 Figure 7 Close up of proglacial discharge and modelled melt and effective rainfall
1033 (precipitation minus evaporation) for each of the different surface types (shown as an area
1034 plot) for a 10 day period of a) Phase 2 in 2010, b) Phase 2 in 2011, c) Phase 3 in 2010 and d)
1035 Phase 3b in 2011. Note that the y-axis has been constrained to 20 m^3 s^{-1} to allow discharge
1036 fluctuations to be seen more clearly.

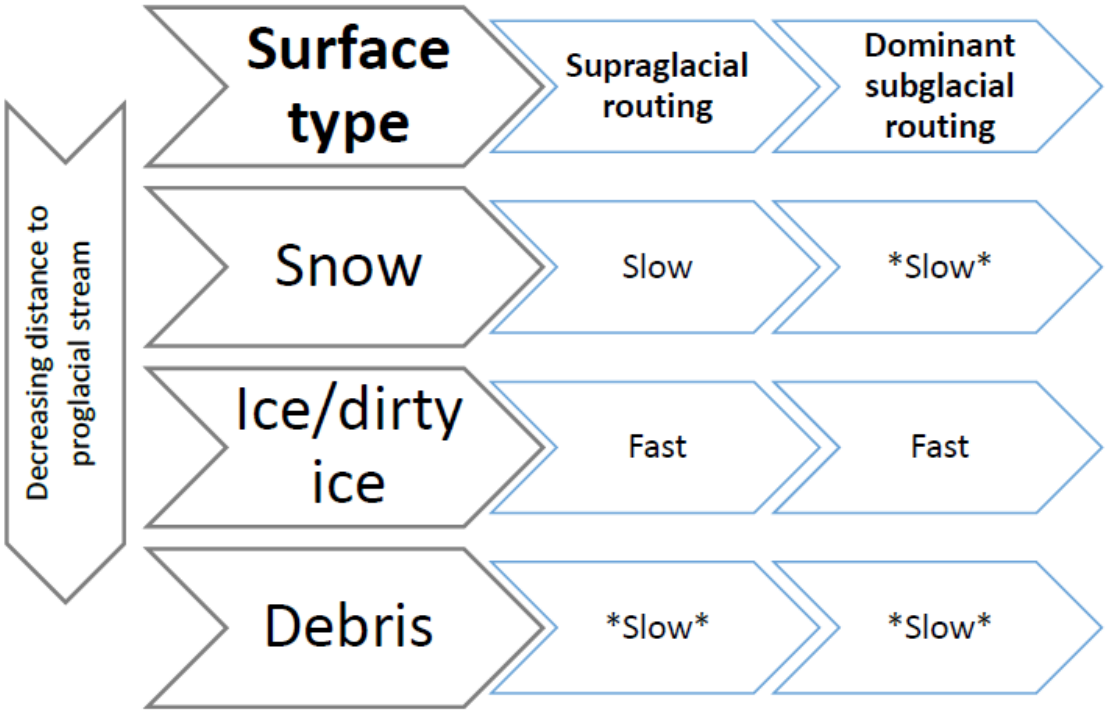

1037

1038 Figure 8 Conceptual diagram of runoff components, and their relative travel time class for a
1039 debris-covered glacier. The stars indicate where solute could be principally acquired by the
1040 meltwater.

1041